Russian Geology and Geophysics © 2019, V.S. Sobolev IGM, Siberian Branch of the RAS
Vol. 60, No. 9, pp. 990–1007, 2019 *DOI:10.15372/RGG2019068* *Geologiya i Geofizika*

Geochemical Events at the Cenomanian–Turonian Boundary: Relation of Anoxia with Volcanism, Climate, and Ocean Circulation

O.L. Savelyeva

Institute of Volcanology and Seismology, Far Eastern Branch of the Russian Academy of Sciences, bul'v. Piipa 9, Petropavlovsk-Kamchatskii, 683006, Russia

Received 22 February 2018; received in revised form 10 December 2018; accepted 5 February 2019

Abstract—The paper presents a detailed review of chemostratigraphic data on the Bonarelli oceanic anoxic event (OAE2) at the Cenomanian–Turonian boundary from different regions worldwide, with a focus on the respective redox conditions in the basins, metal anomalies, and $\delta^{13}C$ excursions. Marine sediments with OAE2 signatures in Eastern Kamchatka are compared with their counterparts from submarine volcanic rises in the northwestern Pacific. The available isotope ages of lavas from some large igneous provinces are correlated with the age of OAE2. The Bonarelli event was triggered and governed by several interrelated factors: volcanism, climate, and ocean circulation. The supply of nutrients into oceans as a result of enhanced magmatism, hydrothermal activity, and weathering on continents played an important role in maintaining anoxia. The spatial patterns of black-shale deposition were controlled by ocean circulation. Geochemical and biochemical processes associated with high productivity ultimately led to its reduction and to the recovery of oxic conditions in oceans.

Keywords: OAE2, carbonaceous rocks, Cenomanian–Turonian boundary, bioproductivity, large igneous province, redox, stable isotopes, ocean circulation

INTRODUCTION

Major events of changes in global climate, biota, and seawater chemistry are important stratigraphic markers. The modern methods of event stratigraphy combined with paleontological constraints allow correlating sedimentary sequences from different oceans. The shortage of oxygen in seas and oceans, known as oceanic anoxic events (OAE) (Schlanger and Jenkyns, 1976), left imprint in sediments. These events, especially numerous in Cretaceous sections, were originally distinguished according to layers of marine black organic-rich sediments deposited in different environments from deep oceans to shallow shelves. Each anoxic event has its features which are related to specific volcanic, climate, and biotic factors and are recorded in the lithology and chemistry of sediments (Orth et al., 1993; Jenkyns, 2010). In this respect, the OAE stratigraphic levels are key objects for studies of paleoclimate and perturbations to the ocean-climate equilibrium.

The OAE2 event at the Cenomanian–Turonian boundary (C/T) is remarkable by fast and voluminous accumulation of organic carbon (C_{org}). It is called the Bonarelli event after Guido Bonarelli (1871–1951) who was the first to describe Upper Cenomanian black shales in the Bottacione and Contessa sections near Gubbio town in the Central Apennines. The Bonarelli level is a regional stratigraphic marker of the Umbria-Marche basin in Central Italy (Luciani and Cobianchi, 1999; Mort et al., 2007b), but the Bonarelli event refers to global-scale increase in black shale deposition (Jenkyns et al., 2007). Sequestration of enormous amounts of lighter ^{12}C isotope rendered ocean waters and atmosphere relatively enriched in ^{13}C and caused a shift toward higher $\delta^{13}C$ (Kuypers et al., 2002; Tsikos et al., 2004; Jenkyns, 2010). The $\delta^{13}C$ signal became recorded in the depositing carbonates and organic matter. The OAE2 level is identified and correlated using carbon isotope compositions combined with data of biostratigraphy and radioisotope dating where possible (Jenkyns et al., 2007), while specific sections may contain different amounts of C_{org}.

This paper presents a synthesis of recent advances in OAE2 chemostratigraphy, with a focus on the evolution of the event: its causes and patterns, and the interplay of its main factors, such as volcanism, climate, ocean circulation, etc. Different models are discussed for ocean circulation and possible causes of climate change at the Cenomanian–Turonian boundary.

GEOGRAPHY OF SECTIONS BEARING OAE2 TRACES

The previous comprehensive overview of sediments that store a record of the Bonarelli event (Schlanger et al., 1987) presented data on lithology and carbon isotope compositions from sections in the regions of Europe, Atlantic, Pacific, and

✉ Corresponding author.
E-mail adress: savelyeva@kscnet.ru (O.L. Savelyeva)

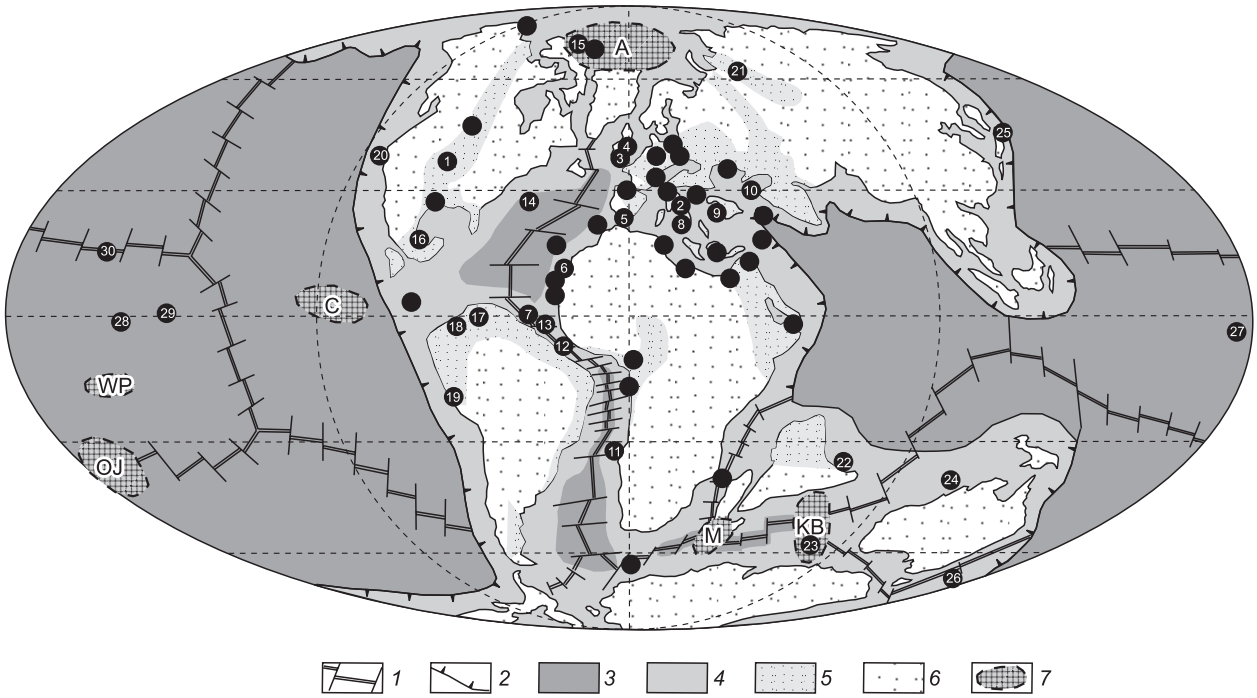

Fig. 1. Mid-Cretaceous paleogeography (90 Ma). *1*, mid-ocean ridges and transforms; *2*, subduction zones; *3*, deep ocean; *4*, shallow ocean; *5*, epicontinental seas; *6*, landmass; *7*, large igneous provinces, with their names abbreviated as C, Caribbean Plateau, OJ, Ontong Java Plateau, WP, West Pacific seamounts, A, Arctic Province, KB, Kerguelen Plateau and Broken Ridge, M, Madagascar Province. Circles mark sections with OAE2 interval inferred from high C_{org} contents and/or $\delta^{13}C$ excursion. Numerals stand for the present position of sections mentioned in the text: 1, Pueblo; 2, Central Apennines (Furlo, Bottacione, Contessa, and Gorgo Cerbara); 3, Eastbourne; 4, South-Ferriby; 5, Manilva (South Spain); 6, Tarfaya (Morocco); 7, Demerara Rise; 8, Sicily; 9, Greece; 10, Caucasus; 11, site 530 DSDP; 12, site 367 DSDP; 13, site 144 DSDP; 14, site 603 DSDP; 15, Axel Heiberg; 16, Mexico; 17, Maracaibo (Venezuela); 18, Columbia; 19, Peru; 20, California (Baden Canyon Formation); 21, northern Siberia; 22, Tibet; 23, Kerguelen Plateau; 24, Exmouth Plateau; 25, Hokkaido Island (Yezo Group); 26, New Zealand; 27, site 585 DSDP (East Mariana basin); 28, site 305 DSDP (Shatsky Rise); 29, site 310 DSDP (Hess Rise); 30, Kamchatsky Mys Peninsula (Eastern Kamchatka). The positions of continents are according to (Scotese, 2004). Compiled with reference to published data (Schlanger et al., 1987; Tarduno et al., 1998; Takashima et al., 2006; Trabucho-Alexandre et al., 2010; Lenniger et al., 2014).

Indian Oceans, North America (Western Interior Seaway, WIS basin), Alaska, Canadian Arctic Archipelago, Central and South America, northern and central Africa. Many of these sections have been documented in detail for three recent decades, and many new sections have been discovered and investigated (Fig. 1), such as site 1260B ODP in the Demerara Rise (Hetzel et al., 2009), site 1138 ODP in the Kerguelen Plateau (Holbourn and Kuhnt, 2002), site S57 and other boreholes in the Tarfaya Basin in Morocco (Kolonic et al., 2005), as well as sections in Egypt (El-Sabbagh et al., 2011), Tibet (Wan et al., 2003; Li et al., 2009; Bomou et al., 2013), Sicily (Scopelliti et al., 2004), Greece (Karakitsios et al., 2007), Caucasus (Levitan et al., 2010; Gavrilov et al., 2013), northern Siberia (Lebedeva and Zverev, 2003), Axel Heiberg Island (Lenniger et al., 2014; Herrle et al., 2015), and in Circum-Pacific orogens (Takashima et al., 2004; Saveliev et al., 2007; Hasegawa et al., 2013; Du Vivier et al., 2015b).

The Pueblo section (Colorado, USA) was chosen as a C/T stratotype that provides reference for OAE2 dating using high-resolution biostratigraphy, $\delta^{13}C$ variations, and isotope ages of bentonite. The sections from West Europe, North America (WIS), North Africa, and North Atlantic Ocean remain the most exhaustively documented. The redox conditions in Late Cenomanian oceans reconstructed for these sections by different methods are briefly characterized below.

DISTRIBUTION OF BLACK SHALES AND OAE2 REDOX CONDITIONS

The bottom water redox conditions (Tyson and Pearson, 1991) are classified as oxic (>2 ml O_2/l H_2O), dysoxic (0.2–2.0 ml O_2/l H_2O), suboxic (0–0.2 ml O_2/l H_2O), anoxic (0 ml O_2/l H_2O), and euxinic (lack of O_2 and predominant H_2S in sediments and water); H_2S may be present in sediments at any depth (Tribovillard et al., 2006).

Biota and concentrations of some biomarkers, as well as redox-sensitive metals and isotope systems, are reliable paleoredox proxies (Pogge von Strandmann et al., 2013). High-quality reconstructions require combining several proxies, especially in the case of using S/C and C/P ratios, degree of pyritization, contents of reactive Fe, or pyrite grain sizes (Meyer and Kump, 2008).

The distribution of some isotopes in section can place constraints on the global extent of anoxic and euxinic conditions during the Bonarelli event. This extent remains controversial: euxinic bottom water during OAE 2 was estimated to occupy ~2.5–7.0% of the seafloor surface, or 15 to 40 times the present value, according to $\delta^{13}C$ and $\delta^{34}S$ modeling (Owens et al., 2013), but U isotope data modeling indicated a smaller extent of anoxic (including euxinic) environments: ~1–2% of the seafloor and three times greater than now (Montoya-Pino et al., 2010). Anyway, most of ocean waters remained suboxic and/or oxic during the event. Organic carbon deposition began in the southwestern North Proto-Atlantic (NPA) Ocean prior to the $\delta^{13}C$ excursion, and then propagated to northern NPA, Tethys (Kuroda and Ohkouchi, 2006) and WIS basins (Mort et al., 2007a) after the excursion.

Data from intervals corresponding to OAE2 show that euxinic settings were widespread mainly in the NPA region where C_{org} was especially abundant (Meyer and Kump, 2008). Laminated organic-rich sediments on the Demerara Rise and in the Tarfaya and Maracaibo basins were deposited from the Late Aptian to the Early Turonian, with the highest C_{org} burial rates during OAE2 (Jenkyns et al., 2007; Martin et al., 2012). Many Atlantic boreholes store evidence of euxinic conditions in the photic zone immediately before and during OAE2 (Sinninghe Damsté and Köster, 1998; Kuypers et al., 2002; Kolonic et al., 2005; Forster et al., 2008; Jenkyns, 2010). On the other hand, euxinic conditions had a larger extent in the south of NPA, where substantial amounts of marine organic carbon accumulated at different depths, than in its northern part where terrestrial organic matter predominated while marine organic-rich sediments were limited to a few layers (Trabucho-Alexandre et al., 2010; Owens et al., 2012). Oxic conditions prevailed in some areas of northern NPA, western Tethys, and WIS (Westermann et al., 2010; Owens et al., 2012; Eldrett et al., 2014) where deposition occurred above the oxygen minimum (Schlanger et al., 1987).

Redox variations during OAE2 (Naidin, 1993; Forster et al., 2008; Gavrilov et al., 2013; Núñez-Useche et al., 2016), as well as alternating prevalent nitrate and sulfate reduction in the water (Jenkyns et al., 2007), are recorded in many North and South Atlantic, Mexican Sea, WIS, western Tethys and Perithetys sections. Redox conditions may have orbital forcing (Sageman et al., 1997; Kuypers et al., 2004a; Mort et al., 2008) which affects the location and strength of trade winds and upwelling in intermediate waters rich in nutrients (Kolonic et al., 2005; Dickson et al., 2016).

The Bonarelli event has been much worse constrained in the Proto-Indian Ocean and in the Eastern Tethys. The available evidence is limited to brief dysoxia reported from the Kerguelen Plateau in the Indian Ocean (Holbourn and Kuhnt, 2002) and predominant oxic or dysoxic conditions recorded in different Tibet sections of the Eastern Tethys (Wan et al., 2003; Li et al., 2009; Bomou et al., 2013). Data from the northwestern margin of Australia indicate black shale deposition on the shelf, within the oxygen minimum zone (site 762 and 763 DSDP in the Exmouth Plateau), and concurrent oxic deposition at greater depths (Thurow et al., 1992).

Sediments with foot prints of anoxia and high C_{org} contents at the OAE2 level are absent from some areas in the Pacific, e.g., in the sections of Peru that were deposited in a back-arc basin (Navarro-Ramirez et al., 2016) or in the Franciscan limestone in California deposited upon oceanic rises at 17° S in the East Pacific (Sliter and Premoli Silva, 1990). Sections in New Zealand include redbeds at the OAE2 level; the taxonomy of micro- and macrofossils changes earlier than in the European sections, before the $\delta^{13}C$ excursion (Hasegawa et al., 2013). Fore-arc sections (Yezo Group in Hokkaido Island or Baden Canyon Formation in California) contain small amounts of terrestrial C_{org} at all depths, but oxygen depletion in the area is questionable. There were reports of oxic conditions during OAE2 in these areas (Nemoto and Hasegawa, 2011; Takashima et al., 2011), but the onset of OAE2 in the Yezo Group section was moved to a zone of greater pyrite contents 22.5 m upwards in a later publication (Du Vivier et al., 2015b). Meanwhile, high C_{org} contents measured within the $\delta^{13}C$ excursion interval corresponding to OAE2 in the Baden Canyon Formation (Magtoto et al., 2014) mean some anoxia. The anoxic event appears only in $^{87}Sr/^{86}Sr$ and $\delta^{13}C$ excursions from site 463 DSDP (Ando et al., 2009) and as a $\delta^{13}C$ excursion in site 869 ODP (Jenkyns et al., 1995).

Deposits rich in organic carbon (9.3–9.9% C_{org}) at the OAE2 level coincide with the $\delta^{13}C$ excursion only in the equatorial Pacific (Owens et al., 2013). They are found redeposited by turbid flows in the East Mariana basin (site 585 DSDP) and occur as thin *in situ* layers among carbonate and siliceous sediments on the Hess and Shatsky Rises (site 305 and 310 DSDP, respectively) (Schlanger et al., 1987). A thin carbon-rich layer (up to 53% C_{org}), lying among carbonate and siliceous rocks in the Kamchatsky Mys Peninsula (Savelyeva et al., 2010), was deposites in a similar setting, at the surface of seamount, possibly within the 20°–30° N paleolatitudes judging by the taxonomic composition of radiolarians (Vishnevskaya, 2001). The relative contents of redox-sensitive elements indicate euxinic conditions in the bottom water (Savelyeva et al., 2010). Note that redbeds in the Tethys and North Atlantic sections commonly appear above OAE2 and are very rare in sediments between anoxic events, whereas the Pacific pelagic sections may contain carbon-rich layers inside redbeds which are composed of red-brown chert and orange chalk in site 305 and of red-brown jasper and pink limestone in the Kamchatsky Mys. Therefore, the Pacific deepwater areas were dominated by oxic conditions which gave way to anoxic and euxinic settings within limited areas and time spells. The black shale deposition on Pacific oceanic rises has been commonly explained by the location of their tops within local zones of oxygen minimum where the sediments could gain C_{org} (Dean et al., 1981).

Thus, the Bonarelli event has been recorded in numerous borehole sections and outcrops in all oceans at different depths and latitudes and in different deposition environments. The deposition was not always accompanied by C_{opr} enrichment: black shales are very unevenly distributed and not perfectly synchronous. The uneven redox conditions during OAE2 resulted from regional or local variations in bioproductivity controlled by basin depth and geometry, ocean circulation, and fluxes of nutrients. These factors are considered below in terms of available knowledge and geochemical models for the respective mechanisms.

ANOMALIES OF TRACE ELEMENTS AT THE OAE2 LEVEL

Sediments deposited in anoxic conditions are commonly enriched in redox-sensitive elements (RSE): As, Sb, Co, Cr, Cu, Mo, Ni, Pb, Zn, Cd, Re, U and V. RSE can accumulate in reduced environments by different mechanisms: precipitation as sulfides or as metal-organic complexes (during early diagenesis), coprecipitation with iron sulfide, scavenging by organic matter, or bioaccumulation (Tribovillard et al., 2006; Turgeon and Brumsack, 2006; Núñez-Useche et al., 2016). On the other hand, high abundances of metals in OAE intervals are often explained by their voluminous inputs to seawater (Trabucho-Alexandre et al., 2010; Núñez-Useche et al., 2016). Additional metal sources are easier to pick when geochemical anomalies have no correlation with organic carbon (anoxia). This is the case of sixteen WIS sections in North America, with one or two closely spaced metal abundance peaks of Sc, Ti, V, Cr, Mn, Co, Ni, Ir, Pt and Au in the upper Cenomanian (Orth et al., 1993); for instance, Ir reaches 0.11 ppm against the local background of 0.017 ppm. As it was shown by further studies of metal anomalies in the Rock Canyon section in Pueblo, Colorado (Snow et al., 2005), the upper peak appears as enrichments in Mn, Ba, Y, Au and Sr about 8 to 20 times the background and in Sc, As, Bi, Ag, Na, Cr, Co, Ni, Cu, Cd, Fe, V, Se, W, Pb, Mg and Ti about 3 to 6 times background values. In the lower anomaly, the concentrations of Mn, Na, Ba, Cr, Co and Sc are 5–7 times and those of Sr, Y, Cu, Ag, W, Ni, Bi, Fe, Se, V, Au, As, Pb, Mg, Ti and Cd are 2–4 times background level; the Co peak is especially prominent (Fig. 2). The anomalies hardly can result from impact events, judging by the absence of microspherules or shock mineral grains, as well as the Sc, Ti, V and Mn enrichments at the level of the Ir peak, which commonly have no relation to meteorites. Continental weathering is also an unlikely cause of the anomalies, given the sharpness of the peaks and far distance of the sections to clastic source areas. The relative abundances of elements in the anomalous intervals similar to those in Hawaiian lavas and MORB rather suggest a volcanic/hydrothermal source of metals (Orth et al., 1993). The lower interval, with weaker anomalies, correlates with the onset of the positive $\delta^{13}C_{org}$ excursion in the beginning of OAE2 in the Rock Canyon section, 4 m below the C/T boundary. The upper interval, with stronger anomalies, lies in the beginning of the $\delta^{13}C_{org}$ plateau (see below), 2 m below the C/T boundary (Fig. 2) (Snow et al., 2005). Both in-

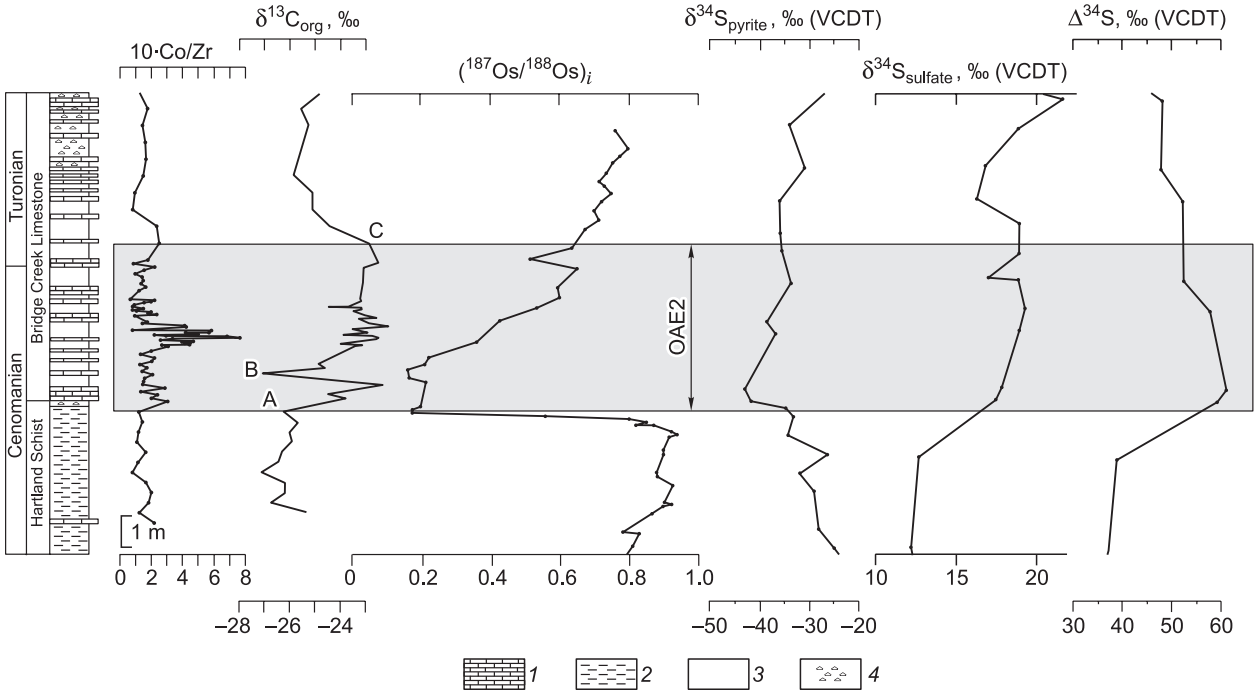

Fig. 2. Synthesis of geochemical data from C/T sections in the Pueblo area (Colorado). Lithology is simplified after (Sageman et al., 2006). *1*, limestone; *2*, limy shale; *3*, marl and limy shale; *4*, lenses of detrital limestone. Co/Zr and $\delta^{13}C_{org}$ curves are after (Snow et al., 2005); $^{187}Os/^{188}Os$ curve is after (Du Vivier et al., 2015b); $\delta^{34}S$ curves are after (Adams et al., 2010). A, B, C are stratigraphic levels.

tervals span ca. 120 kyr, which fits the duration of a volcanic event. The respective sediments are enriched in less volatile and more reactive elements (Sc, Co, Mn, Fe) and have lower contents of more volatile and less reactive Se, Cd, W, Au, and Bi, which is evidence of proximity to the metal source (Snow et al., 2005). The upper anomaly in the Pueblo rocks corresponds to a Cr/Al peak in the Eastbourne section within the lower *Whiteinella archaeocretacea* zone in the end of the Plenus cold event (Pearce et al., 2009).

A double Ir peak (up to 0.56 ppm, relative to carbonate-free material) similar to that in the WIS sections, as well as peaks in Sc, Ti, Cr, Fe and Hf and two additional metal anomalies up- and down section, were discovered in southern Central Columbia in Upper Cenomanian black shale (Orth et al., 1993). The same authors found intervals of high metal abundances in numerous C/T boundary sections worldwide (Orth et al., 1993): from Europe (England, Germany, Poland), Atlantic and Pacific (ODP/DSDP cores) areas, though with much smaller peaks than in WIS and Columbia. Therefore, the source(s) of metals may occur in the Proto-Caribbean, Gulf-of-Mexico, or eastern Pacific regions.

The geochemical anomalies at the C/T boundary were possibly associated with the origin of metal-saturated hydrothermal plumes during the formation of the Caribbean Plateau in the Eastern Pacific 5000 km far from the WIS area (Sinton and Duncan, 1997; Snow et al., 2005). In this case, metal anomalies would be detected also in the latest Cenomanian sediments of equatorial Pacific, but the DSDP 585 core and Franciscan limestone samples show only weak metal enrichments above the local background. Specifically, small peaks of Sc, Ti, V, Cr and, possibly, Ir in the site 585 cores from the East Mariana basin (paleolatitude 6° S), at the contact of sections 2 and 3, or 72 cm above the organic-rich layer are found (Orth et al., 1993). Note in this respect the high contents of some elements in Upper Cenomanian black shale from the Kamchatsky Mys Peninsula that was deposited on a submarine volcanic rise in an open ocean (Savelyeva et al., 2015). They are Cu, Ni, Zn, Ba, V, Mo, U, and Ti (including Al-normalized) enrichments relative to the host jasper and limestone, as well as high concentrations of Au, Ag, PGE, and Re; the mineral component of the rocks contains 3.08 ppm Ir and 2176 ppm Pt (Savelyeva et al., 2015). The enrichment may be due to deposition in euxinic conditions. On the other hand, ash of carbonaceous rocks contains more Al, Ti, Mg, K and Zr than the jasper and limestone hosts, which suggests a contribution of some other most likely volcanic source mixed with the background clastics and clay particles (Savelyeva et al., 2015). Some elements in the organic-rich sediments that deposited in a euxinic environment came from proximal and/or distant volcanic and hydrothermal sources. In general, the distribution of metals near the C/T boundary within the Pacific region remains poorly investigated.

The metal flux into sediments in closed marine systems may exceed that from a source associated with deep water renewal (Tribovillard et al., 2006). The OAE2 intervals in sections from such basins may contain lower concentrations of some elements as a result of the respective seawater depletion. For instance, Mo, V and Zn fall to the minimum values approaching the concentrations in the crust within the $\delta^{13}C$ plateau in the Demerara Rise where organic carbon accumulated in sediments before, during, and after the anoxic event (Owens et al., 2016). Note that V decreases before the positive $\delta^{13}C$ excursion, which records a global expansion of oxygen-depleted (but not sulfide) waters. The Mo decrease (low Mo/C_{org} ratios) coincides with the onset of OAE2 and reflects a global expansion of euxinic waters, global-scale Mo deposition and, hence, the depletion of the global Mo reservoir. Low Mo/C_{org} ratios were also reported from numerous C_{org}-rich OAE2 sections in WIS, North and South Proto-Atlantic, and Tethys areas.

Thus, metal abundance anomalies near the C/T boundary have implications for redox environments on both local and global scales, as well as in specific North America, Columbia, Europe, Atlantic, and Pacific sections. The redox conditions in these sections correspond to volcanic and hydrothermal activity in the latest Cenomanian, including two large magmatic events immediately before OAE2 and in the beginning of the $\delta^{13}C$ plateau.

ISOTOPE STRATIGRAPHY OF OAE2 INTERVAL

Sections with OAE intervals are commonly studied with reference to isotope signatures sensitive to variations in hydrothermal inputs into basins, weathering rates, and redox conditions. The $\delta^{13}C$ excursion at the OAE2 level (Arthur et al., 1988) coexists in marine sections with distinct signals of Li (Pogge von Strandmann et al., 2013), Nd (MacLeod et al., 2008), Os (Du Vivier et al., 2014, 2015b; Turgeon and Creaser, 2008), Pb (Kuroda et al., 2007), Sr (Ando et al., 2009; Bralower et al., 1997; Jones and Jenkyns, 2001), U (Montoya-Pino et al., 2010), S (Adams et al., 2010; Owens et al., 2013), Ca (Blättler et al., 2011; Du Vivier et al., 2015a), Fe (Owens et al., 2012), and Cr (Holmden et al., 2016; Wang et al., 2016) isotopes. These elements come from different sources and have different residence times in ocean water, estimated with regard to the ~1000 year water renewal cycle (Broecker and Peng, 1982), though the residence times of some elements in the Cretaceous may have been different from the present values (Snow et al., 2005). The available data for isotopes of different elements are more or less abundant and reliable, and the most consistent results are presented below. The carbon isotope composition is the best documented.

C isotope composition. The ca. 150 kyr long residence time of carbon in seawater (Owens et al., 2013) ensures its homogeneous isotope composition over prolonged time spans. The Bonarelli event associated with global-scale black shale deposition perturbed significantly the carbon cycle and involved both the ocean and the atmosphere (Tsikos et al., 2004; Jarvis et al., 2006). The event appears

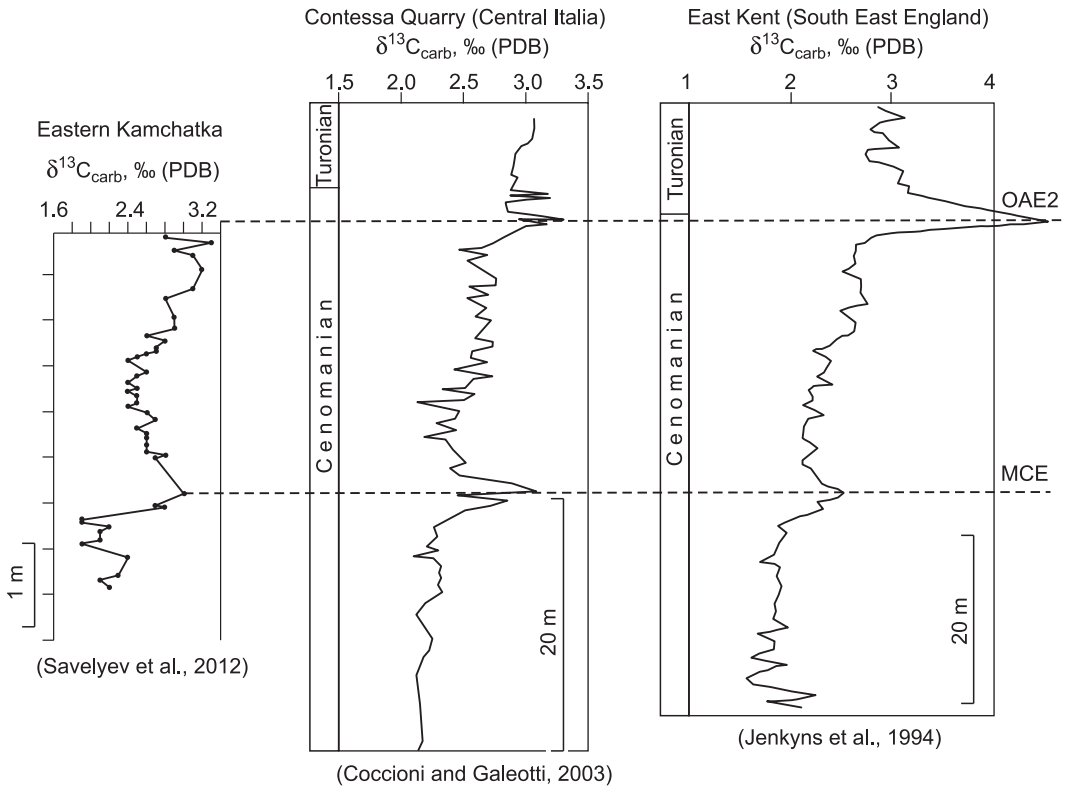

Fig. 3. Fragments of typical $\delta^{13}C_{carb}$ curves in the interval from MCE to OAE2.

globally as a distinct positive $\delta^{13}C$ excursion of ~2–3‰ in marine carbonates and terrestrial organic matter and ~4–6‰ in marine organic matter (Jenkyns et al., 2007). The excursion results from ^{12}C depletion of CO_2 reservoirs as a result of large-scale burial of organic carbon (Arthur et al., 1988). The $\delta^{13}C_{org}$ and $\delta^{13}C_{carb}$ stratigraphy allows identifying OAE2 intervals and provides reference for other isotope systems at the respective level. The magnitude of the $\delta^{13}C$ excursion varies according to local variations in the C_{org} burial rate, and is 2‰ greater than elsewhere in the southern NPA area where enormous amounts of black shale were deposited during OAE2 (Arthur et al., 1988; Jenkyns et al., 2007; Jarvis et al., 2011). The $\delta^{13}C_{carb}$ patterns between the Middle Cenomanian isotope event (MCE) and OAE2 are similar in many Paleopacific and Tethys sections: in Kamchatka (Savelyev et al., 2012), Italy (Coccioni and Galeotti, 2003), England (Jenkyns et al., 1994), and others (Fig. 3).

The onset of OAE2 corresponds to the base of the positive $\delta^{13}C$ excursion. The sections are commonly correlated against the stratigraphic levels A, B and C in the $\delta^{13}C$ curve. The level A represents the last relatively depleted $\delta^{13}C$ before the first significant shift toward positive values, B marks a small interval of depleted $\delta^{13}C$ after the positive excursion, and C refers to the last relatively enriched $\delta^{13}C$ before it turns back to the pre-OAE2 values (Tsikos et al., 2004; Du Vivier et al., 2015b) (Fig. 2). Some models include two Late Cenomanian $\delta^{13}C$ highs separated by a small low corresponding to the Plenus cold event. The peaks are followed by a plateau (continuously high $\delta^{13}C$) in relatively shallow-water sections like Eastbourne or Pueblo or by a rapid decrease in deeper water (Manilva and Furlo). The second $\delta^{13}C$ peak is often poorly pronounced in deep-water sections. The difference may be due to changes in regional productivity or deposition gaps (Tsikos et al., 2004; Mort et al., 2007c). The OAE2 interval in the Pueblo C/T stratotype section (Colorado) has a sharp beginning but a smooth and hardly detectable end. Therefore, even in the stratotype the radioisotope dating of bentonite beds and astrochronology give considerably different estimates of OAE2 duration. According to recent available dates, the positive $\delta^{13}C$ excursion lasted ~600 kyr (Tsikos et al., 2004; Sageman et al., 2006) and OAE2 in the Peublo section began at ~94.38 ± 0.15 Ma (Meyers et al., 2012). The event in the Hokkaido Yezo Group section has the same duration of 600 kyr and the onset at 94.44 ± 0.14 Ma according to U–Pb zircon ages of tuff layers, along with carbon and osmium isotope data. Thus, the OAE intervals appear synchronously in the WIS and Japan sections (Du Vivier et al., 2015b).

There were reports of a short negative excursion in the $\delta^{13}C_{org}$ and $\delta^{13}C_{carb}$ curves for sections in Central Italy, southern England, southeastern North Atlantics, Japan, and WIS (Kuroda et al., 2007). It may be due to ^{12}C inputs into the ocean–atmosphere system with CO_2 released from the mantle by volcanic degassing or CH_4 liberated from gas hy-

drates. A similar brief low was revealed in the Tappu section in Hokkaidao (Nemoto and Hasegawa, 2011) and was cautiously correlated to negative excursions in other sections worldwide. Nemoto and Hasegawa (2011) presumed that the low might correlate with $\delta^{13}C_{org}$ excursions in the sections of Gorgo Cerbara (Central Italy), Eastbourne and Pueblo.

The $\Delta^{13}C$ difference between $\delta^{13}C$ values of carbonate and marine organic matter is another marker besides $\delta^{13}C$ in event stratigraphy. It is a good p_{CO_2} proxy (Jarvis et al., 2011): isotope fractionation by phytoplankton accelerates at increasing atmospheric CO_2 partial pressure and greater CO_2 availability in surface water, whereby ^{13}C shifts to more negative values. $\delta^{13}C$ of different phytoplankton components can be used for the same purpose (Sinninghe Damsté et al., 2008). As applied to OAE2, thus reconstructed p_{CO_2} increased in the Late Cenomanian, decreased during the first $\delta^{13}C$ peak and then again increased progressively till the Early Turonian. The same pattern is observed in many sections worldwide.

The $\delta^{13}C$ curves of terrestrial organic matter can differ from those for carbonates due to various local or global effects, especially terrestrial vegetation (Kuypers et al., 1999). For instance, $\delta^{13}C$ of terrestrial C_{org} in Japan show a negative trend all over the Cenomanian, possibly, because of higher climate humidity and thick forest coverage. In the conditions of shadow photosynthesis, $\delta^{13}C$ in leaves has a prominent vertical gradient leading to lower $\delta^{13}C$ values of organic products (Hasegawa, 2003).

In general, carbon isotope data can make basis for detection and worldwide tracing of the OAE2 level.

Sr isotope composition. The Sr isotope composition of ancient oceans left imprints in carbonate and phosphate sediments. Sr has homogeneous isotope ratios at any period, as its residence time (~5 Myr) is much longer than water renewal cycles (Snow et al., 2005). The $^{87}Sr/^{86}Sr$ database for well preserved and reliably dated marine sediments was used to plot and update the respective curve for the past 590 Myr of the geological history (McArthur et al., 2012). In the latest Cenomanian, the $^{87}Sr/^{86}Sr$ curve begins to shift to lower (unradiogenic) values approximately near the OAE2 level. The negative excursion is much broader than the OAE2 interval, due to longer Sr residence time in seawater. The $^{87}Sr/^{86}Sr$ ratios are the lowest in the Turonian and return to the previous values in the Santonian. The low means that the hydrothermal Sr input ($^{87}Sr/^{86}Sr \approx 0.703$) at that time exceeded the continental flux, with $^{87}Sr/^{86}Sr \approx 0.712$ (Bralower et al., 1997). The isotope shift may have three possible causes: (1) reduction of river Sr input from weathered continental crust; (2) $^{87}Sr/^{86}Sr$ decrease in river waters; (3) ^{86}Sr input from submarine hydrotherms. The third scenario appears the most probable according to modeling with regard to the history of seawater temperatures, sealevel, land surface area, and volcanism in oceanic plateaus and mid-ocean ridges (Jones and Jenkyns, 2001). The sources of excess ^{86}Sr were attributed either to intraplate volcanism, specifically that of Caribbean Plateau for the case of OAE2 (Snow et al., 2005), or to hydrothermal systems of mid-ocean ridges (MOR) at the time of faster seafloor spreading, given that the curve shape departs from the intraplate volcanic trend (Bralower et al., 1997; Jones and Jenkyns, 2001), or to both (Jenkyns, 2010). The coincidence of the $^{87}Sr/^{86}Sr$ excursion with black shale deposition interval may result from a causative relation between mantle plume volcanism and OAE2 (Sinton and Duncan, 1997; Leckie et al., 2002; Snow et al., 2005). However, the $^{87}Sr/^{86}Sr$ shift began >0.6 Myr before OAE2, i.e., volcanism and the ensuing global change may have prepared the climate and oceanic regimes to OAE2 but did not trigger it directly (Jones and Jenkyns, 2001; Ando et al., 2009).

Some sections contain a brief ^{87}Sr peak in the beginning of OAE2 standing against the general $^{87}Sr/^{86}Sr$ decrease, possibly related to rapid weathering of silicates during accelerated hydrological cycles (Frijia and Parente, 2008; Jenkyns, 2010; Jarvis et al., 2011).

Os isotope composition. The Os isotope composition of seawater records the mixing of ^{187}Os from weathering old continental crust ($^{187}Os/^{188}Os \approx 1.4$) and ^{188}Os from mantle, hydrothermal, and extraterrestrial sources ($^{187}Os/^{188}Os \approx 0.12$). The short residence time of osmium in seawater (within 10 kyr) allows global OAE2 correlation on the basis of its isotope composition. The $^{187}Os/^{188}Os$ profile is very similar in sections from different regions and settings worldwide: spreading proto-Atlantic Ocean, European pelagic shelf, WIS in North America, Japan forearc basin (Yezo Group), or continental margin in California (Baden Canyon Formation). The $^{187}Os/^{188}Os$ ratios are relatively radiogenic (~0.55–1.00) before OAE2, then shift rapidly to unradiogenic values (~0.20–0.30) ca. 23 kyr before OAE2 (positive $\delta^{13}C$ excursion), and then return to higher values (~0.70), commonly after the B level of the $\delta^{13}C$ curve. This trend in the beginning of OAE2 requires a 30- to 50-fold increase of ^{188}Os flux into oceans, possibly, due to volcanism in large igneous provinces (Turgeon and Creaser, 2008; Du Vivier et al., 2014, 2015b).

The $^{187}Os/^{188}Os$ ratios are more radiogenic around 80 kyr before OAE2 in sections with significant continental clastic inputs (Yezo Group, Baden Canyon, and especially WIS), than in open ocean sections (Du Vivier et al., 2014, 2015b) (Fig. 2). The $^{187}Os/^{188}Os$ profiles in intervals before OAE2 near continents had several controls: enhanced weathering, changes in sealevel and basin openness, and volcanism in large igneous provinces. In the beginning of OAE2, the ^{188}Os input became the predominant factor and caused the similarity of $^{187}Os/^{188}Os$ profiles in C/T sections all over the world (Jenkyns, 2010; Du Vivier et al., 2014). In Pacific sections, ^{188}Os increased at 94.44 ± 0.14 and 94.28 ± 0.25 Ma, around the OAE2 onset (Du Vivier et al., 2015b).

Nd isotope composition. Neodymium has a short residence time in seawater (about 500 years), and its relative inputs from old continental and recent volcanism source differ from basin to basin, which makes it a good proxy of paleoocean circulation. Marine Nd isotope ratios are expressed

as ε_{Nd} (Pucéat, 2008). Fish fossils (phosphate teeth and bones) store a record of seawater ε_{Nd} as they adsorb Nd from the ambient water while depositing on the bottom and are stable to later diagenetic alteration (Zheng et al., 2013).

Nd isotope data are insufficient for complete reconstruction of the Cretaceous ocean circulation, but ε_{Nd} values of that time are known to be the highest for the Pacific (0 to –6), Proto-Atlantic, and Proto-Indian (from –4 to –11) oceans and the lowest (to –18) in the Demerara Rise (Moiroud et al., 2013). The high Nd isotope ratios were due to erosion of island arcs and volcanism in the Pacific, while Nd inputs from weathered continental crust were more important in the other cases.

The ε_{Nd} variations over the OAE2 interval are the best studied in Atlantic sections. In site 1050 ODP, they are close to the respective Pacific ε_{Nd} values and then become common to the Late Cretaceous Atlantic and Tethian ratios (MacLeod et al., 2008). The ε_{Nd} curve for the Demerara Rise includes two positive excursions: one at the base of OAE2, before the positive $\delta^{13}C$ shift, and the other in the middle of OAE2 within a cold spell (Zheng et al., 2013). The excursions may results from (1) reduction of regional continental clastic fluxes or ε_{Nd} changes in the shed material; (2) inputs from a new source with unusual ε_{Nd} values, e.g., volcanic eruptions in large igneous provinces; (3) changes in ocean circulation (MacLeod et al., 2008). The first scenario is unlikely as the first ε_{Nd} excursion correlates with a spell of warm climate and enhanced continental sediment transport (Martin et al., 2012) indicated by data on other (e.g., Sr) isotope systems (Jarvis et al., 2011). Furthermore, continental margins with high ε_{Nd} were absent from the Atlantic region during OAE2. Two other mechanisms have been interpreted in different ways. One model implies that waters with radiogenic ε_{Nd} from the Tethys and North Atlantic Ocean replaced those with unradiogenic ε_{Nd} values typical of the Demerara Rise during OAE2 (Martin et al., 2012). This occurred either because of accelerated evaporation and deep water renewal in the Tethys region or dilution of the South American strait between continents and bottom water density decrease in the Demerara area. Another model attributes inputs of radiogenic Nd to two pulses of volcanism, possibly, in the Arctic or Caribbean large igneous provinces (Zheng et al., 2013). It however remains unclear whether volcanogenic Nd could travel long distances. Long transport was possible only with anoxic waters: otherwise Nd would have been bound in Fe and Mn oxides near the source. The volcanic origin of the positive ε_{Nd} excursion is supported by the presence of layers with high trace metal abundances in North Atlantic marine sections (Orth et al., 1993; Pearce et al., 2009).

S isotope composition. Sulfur fluxes into the ocean are maintained by weathering of continental rocks that bear sulfide and sulfate minerals, as well as by volcanism and hydrothermalism. The fluxes vary in time and space but the $\delta^{34}S$ signatures are similar and confined to a narrow range of 0–8‰ (Owens et al., 2013). Currently $\delta^{34}S$ is about 6‰ in river water and 3–3.5‰ in hydrotherms (Adams et al., 2010). Sulfur has ~2 Myr residence in ocean water (Owens et al., 2013) and escapes by precipitation and burial of gypsum or other sulfates, organic compounds, and pyrite. The S isotope fractionation is the greatest during pyrite formation: sulfate-reducing bacteria reduce sulfate to hydrogen sulfide and enrich the latter with ^{32}S, while the residual sulfate reservoir gains ^{34}S and the precipitating pyrite becomes gradually ^{34}S-enriched at a rate inversely proportional to the concentration of sulfate in seawater. Therefore, the isotope difference $\Delta^{34}S$ between sulfate and sulfide sulfur ($\delta^{34}S_{sulfate} - \delta^{34}S_{pyrite}$) is greater at higher contents of sulfate.

The $\delta^{34}S$ values of sulfates that replace carbonate ions in the carbonate structure and/or $\delta^{34}S$ of pyrite, as well as calculated $\Delta^{34}S$, are common stratigraphic markers. Different sections in North America (WIS), central and southern Italy, and England contain positive $\delta^{34}S_{sulfate}$ excursions at the OAE2 level (Ohkouchi et al., 1999; Adams et al., 2010; Owens et al., 2013), which are consistent with rapid burial of pyrite precipitated in euxinic conditions. The C isotope peak is several hundreds of thousand years ahead of the S one. Modeling of the observed $\delta^{13}C$ and $\delta^{34}S$ excursions predicts 15–40 times faster S burial during OAE2 than at present. The extent of euxinic bottom waters during OAE2 was 15–40 times larger correspondingly, and covered ~2.5–7% of the seafloor (Owens et al., 2013).

Around 500 kyr before OAE2, $\delta^{34}S_{sulfate}$ in the Peublo WIS section decreases to ~5‰, while $\Delta^{34}S$ increases to maximum in the beginning of the OAE2 interval and then decreases during the event (Adams et al., 2010) (Fig. 2). These trends were explained by additional sulfate inputs from a volcanic/hydrothermal source (Adams et al., 2010; Owens et al., 2013), which are consistent with the trends of $\delta^{34}S_{pyrite}$ in the Demerara Rise (Hetzel et al., 2009), WIS (Adams et al., 2010), Tarfaya (Poulton et al., 2015), and Mexico (Núñez-Useche et al., 2016) sections: decrease at different levels before and during OAE2 and gradual increase after the event. Note that sulfate inputs may also result from accelerated continental weathering. Modeling shows that the contents of sulfate required for an isotopic shift may come from greater volcanic or weathering (or both) S inputs (Poulton et al., 2015).

Fe isotope composition. Iron oxide phases become reduced in oxic and suboxic shelf environments, along with diagenetic remineralization of carbon, whereby mainly light iron isotopes release into pore and bottom waters while the residual sedimentary iron, correspondingly, acquires higher $\delta^{56}Fe$. Light Fe migrates in the dissolved form and incorporates into precipitating pyrite in euxinic environments.

Thus, the Fe/Al ratio decreases and $\delta^{56}Fe$ increases in the absence of large hydrothermal inputs in oxic conditions but, on the contrary, Fe/Al increases and $\delta^{56}Fe$ decreases in euxinic settings. The same markers work to reveal hydrothermal and clastic inputs. Sediments that contain hydrothermal Fe have a narrow range of $\delta^{56}Fe$ values around the average for igneous rocks (~0 to 0.5‰) but a large range of elevated

Fe/Al ratios much higher than 0.5 (Owens et al., 2012). In the case of a clastic input, the Fe/Al ratio is about 0.5, i.e., an average for continental crust (Taylor and McLennan, 1995).

Applied to data from the Tarfaya and Eastbourne basins and some NPA borehole sections, these criteria reveal Fe inputs from different sources within the OAE2 interval, as well as iron fluxes from oxic shelf settings in the northern part of NPA to highly productive anoxic shelves of its southern near-equator parts. Furthermore, evidence of high hydrothermal Fe input was inferred for the southern NPA area associated with fast spreading or volcanism in large igneous provinces (Owens et al., 2012).

U isotope composition. The $^{238}U/^{235}U$ ($\delta^{238}U$) ratio is a paleoredox proxy and can be used for estimating the extent of past marine anoxia settings. The flux of U into oceans is maintained by continental weathering and its burial in sediments is associated with isotope fractionation of ^{238}U and ^{235}U. The fractionation is especially high (up to ~1‰ $\delta^{238}U$) in anoxic environments and much weaker in oxic and suboxic conditions and in hydrothermal deposits: heavy isotopes become buried in sediments during reduction of U in anoxic and euxinic conditions, while the light ones remain dissolved.

The present residence time of U in seawater is ~500 kyr and most of uranium precipitates in dysoxic conditions. During OAE2 event, however, uranium burial occurred mainly in anoxic and euxinic environments, and the C/T black shales have more depleted U isotope compositions than their present counterparts (Montoya-Pino et al., 2010). The amount of uranium buried in anoxic sediments during OAE2 on the Demerara Rise was about three times that in the modern organic-rich sediments (Montoya-Pino et al., 2010). Correspondingly, the extent of C/T anoxic and euxinic settings was at least three times greater than at present and could reach ~1–2%.

Thus, variations in isotope ratios of different elements at the Bonarelli level are often interpreted as indicators of increased magmatic and hydrothermal activity. This appears especially reasonable for the isotope systems of Sr and Os and, possibly, Fe, while the ε_{Nd} and $\delta^{34}S$ excursions rather have other explanations. Note that reliable interpretation of the Nd isotope patterns requires data from a greater number of C/T sections. Smaller peaks of radiogenic Sr and, possibly, also $\delta^{34}S$ shifts, may record acceleration of continental weathering in the beginning of OAE2.

AGE OF VOLCANISM IN SOME LARGE IGNEOUS PROVINCES

Inasmuch as chemostratigraphic data often indicate relation of the Bonarelli event with volcanism, the presumed dates of the OAE2 onset around 94.38 ± 0.15 Ma (Meyers et al., 2012) and 94.44 ± 0.14 Ma (Du Vivier et al., 2015b) can be compared with the ages of rocks in different igneous provinces.

Ontong Java Plateau. Manihiki, Ontong Java and Hikurangi formed jointly as a single large superplateau 125 Ma ago and were later separated by spreading (Nakanishi et al., 2015). The age of basalts was determined in samples retrieved by dragging from DSDP and ODP sites and in rocks sampled from obducted blocks in the Solomon Islands. The history of the Ontong Java Plateau comprised two major magmatic events at 122 ± 3 and 90 ± 4 Ma (the former event much larger than the latter one) and a few later episodes (Mahoney et al., 1993, 2001; Tejada et al., 1996). Volcanism did not stop between 122 and 90 Ma, judging by Middle Cenomanian to Coniacian ages of a volcaniclastic interval in site 288 DSDP and Aptian–Albian ages of similar rocks in site 289. Other available ages for this interval are 93.6 Ma, or close to the onset of OAE2, for a fresh feldspar monofraction from site 803 (Mahoney et al., 1993) and Albian to Late Cenomanian ages of calcareous ichnofossils from limestone between lava flows in the upper 15 m of site 1185 ODP, i.e., eruptions continued between ~93 and 112 Ma.

Caribbean Province. The rocks involved in the formation of the Caribbean Plateau are currently exposed in Haiti Island, in orogenic complexes of northwestern South America, and in the surrounding areas of Central America and have been found in DSDP boreholes in the Caribbean Sea. Igneous complexes along the Pacific coast of Central America (Costa Rica) are also assigned to the Caribbean province. The greatest part of the igneous base of Costa Rica is composed of rocks with Ar–Ar ages of 95 and 75 Ma (Hauff et al., 2000). The available Ar–Ar dates for Haiti are close to the OAE2 onset: 95.12 ± 1.44, 94.36 ± 0.63, and 94.43 ± 0.66 Ma (Snow et al., 2005). The major event of flood basalt volcanism in the province occurred between 94.7 and 83.2 Ma, but the whole time span of volcanic activity in the Caribbean Province may extend from 69 to 139 Ma, as younger and older ages of rocks were also obtained (Hoernle et al., 2004). In this respect, Hoernle et al. (2004) inferred that the igneous complexes represented several plateaus and remnants of the Galapagos hotspot which were accreted during subduction.

Western Pacific seamounts. In addition to the Ontong Java and Carribbean Provinces, Middle Cretaceous Pacific intraplate magmatism has been recorded in some oceanic rises (seamounts) located in the Western Pacific region. Middle Cretaceous to Paleogene ages of basalts were obtained for samples from the Magellan (~121 to ~74 Ma), Marcus Wake (~122 to ~63.5 Ma), and northern Marshall Islands (~140 to ~30 Ma) seamounts (Sedov et al., 2005 and references therein). Some of these dates are very close to the onset of OAE2. The site 872 ODP near the Marshall Islands strips Lower Santonian sediments over basalt, which mark the end of volcanism specifically at Lo-En (Hess) guyot (Premoli Silva et al., 1993). In the Kamchatsky Mys Peninsula (East Kamchatka), lava flows and hyaloclastics intercalate with Albian–Cenomanian pelagic jasper and limestone deposited on a volcanic rise in the central Pacific. The hyaloclastic layer lying immediately over the carbon-rich layer

corresponding to OAE2, as well as the presence of a minor volcanic component in the carbonaceous layer, record volcanic activity of the respective age (Savelyeva, 2009). Alkali basalts and enriched tholeiites geochemically similar to the rocks of Detroit seamount evidence that the ophiolites of the peninsula formed under the effect of the Hawaian mantle plume (Savelyev, 2004; Portnyagin et al., 2008).

Arctic Province. Evidence of magmatic and hydrothermal activity in the Arctic Province can be found in the Svalbard and Franz Josef Land islands and in the adjacent shelf, in the Axel Heiberg and Elsmere islands and, possibly, in North Greenland (Tarduno, 1998). Magmatism in the province was a long-lasting event and included two phases with eruptions of tholeiitic (130–80 Ma) and alkaline (85–60 Ma) magmas. The formation of tholeiites was associated with the opening of the Canada basin, possibly, with some participation of a mantle plume. The youngest tholeiite magmatism (100–80 Ma, mostly Cenomanian and Turonian ages and some Campanian dates) was restricted to the northern Canada Archipelago (Tegner et al., 2011). An age close to the OAE2 onset (95.3 ± 0.2 Ma) was obtained for Axel Heiberg island (Tarduno, 1998).

Kerguelen Plateau and Broken Ridge. The available data for this large igneous province are from ODP sites (Frey et al., 2003). The history of the Kerguelen Plateau that formed after the India–Antarctica breakup is recorded by volcanics younging northward from ~119 Ma in the southern part of the Kerguelen Plateau to ~34 Ma in the north, with peaks of magmatism at 119–110 and 105–95 Ma (Ar/Ar ages). The greatest part of the province territory was above the sealevel till the earliest Cenomanian. The Broken Ridge formed from ~100 to ~95 Ma and bordered the central part of the plateau till the Eocene.

Madagascar Province of continental flood basalts. Abundant Late Cretaceous basalt and rhyolite lavas in Madagascar may trace the Marion hotspot which was located beneath the southeastern part of the island at that time. The magmatism (mainly subaerial volcanism) was induced by Madagascar rifting off India. Previous K–Ar dates gave a large range of ages from 31 to 97 Ma, but more precise Ar–Ar determinations showed that the event which produced lavas and dikes in the island's eastern rift margin lasted no more than 6 Myr, with the oldest age 90.7 Ma and a weight average age of 87.6 ± 0.6 Ma (Storey et al., 1995). The range extends slightly at the account of the 91.6 ± 0.3 Ma U–Pb zircon-baddeleyite age of rocks from northeastern Madagascar (Torsvik et al., 1998). However, the volcanic base of the elongate submerged Madagascar Ridge remains unsampled and undated (Kuroda et al., 2007).

Thus, the onset of the Bonarelli event was concurrent with moderate volcanism in the Ontong Java Plateau between two major peaks of activity. Eruptions on some seamounts in the western Pacific occurred within a large time span that encompassed the Late Cenomanian. The onset of OAE2 was shortly preceded by the beginning of voluminous flood basaltic magmatism in the Caribbean Province and the end of a large event in the Kerguelen Plateau–Broken Ridge Province, which were also concurrent with active tholeiitic magmatism in the Arctic Province (from the earliest Cenomanian to the Campanian). Volcanism in the Madagascar Province began in the Turonian, but reconstructing the history of eruptions is often difficult because of poor exposure. Thus, the time span of magmatism in Madagascar and in other provinces is yet to be updated.

RELATION OF THE BONARELLI EVENT WITH VOLCANISM

The role of volcanism in large igneous provinces and related hydrothermal activity in the origin of OAE and the synchroneity of these events have been discussed in many publications (Larson, 1991; Orth et al., 1993; Sinton and Duncan, 1997; Jones and Jenkyns, 2001; Leckie et al., 2002; Snow et al., 2005; Kuroda et al., 2007; Turgeon and Creaser, 2008; Adams et al., 2010; Du Vivier et al., 2014, 2015b). Large eruptions had different consequences: (1) CO_2 emission to the atmosphere and climate warming that accelerated weathering and, hence, inputs of nutrients into oceans (Jones and Jenkyns, 2001; Jenkyns, 2010; Pogge von Strandmann et al., 2013); (2) hydrothermal oceanward transport of reduced metals and sulfides which oxidized by consuming dissolved oxygen and became nutrients for phytoplankton (Sinton and Duncan, 1997; Zheng et al., 2013); (3) volcanic upwelling that carried more nutrients to the water surface (Price, 2003). The increasing availability of biolimiting nutrients and CO_2 stimulated primary productivity, whereby much oxygen became spent on decomposition of organic matter while anoxia occupied large oceanic areas (Bralower, 2008; Trabucho-Alexandre et al., 2010).

The specific mechanisms of environment forcing by volcanism in the latest Cenomanian are open to discussion. It remains unknown which is the key control of bioproductivity: input of nutrients into oceans directly from volcanoes and hydrotherms or fluxes from the land maintained by accelerated hydrological cycles and weathering. In some models, nutrients are considered to result from rock-water interaction reactions during hydrothermal alteration of oceanic flood basalts (Snow et al., 2005). However, the description and quantitative estimates of hydrothermal systems associated with volcanism in oceanic plateaus remain hypothetical for the lack of modern analogs. Eruptions may have produced metal-loaded hydrothermal plumes, most likely anoxic. The plumes, moving in low-pH seawater, entrained metals and carried them to long distances (Trabucho-Alexandre et al., 2010; Holmden et al., 2016) from eruption centers in the Pacific and Indian Oceans and in the northern polar area. Nd isotope data indicate that intermediate water masses may have penetrated from the Pacific through the Central American strait (MacLeod et al., 2008; Zheng et al., 2013) and delivered metals to NPA and southern WIS. The WIS basin was presumably located relatively close to the

Caribbean Province and was exposed to effects from mantle plumes and magmatic degassing, which is consistent with high contents of both volatile and nonvolatile elements within the OAE2 interval in the Rock Canyon section (Snow et al., 2005). According to some interpretations (Kuroda et al., 2007), the global spread of volcanic products in the latest Cenomanian was possibly due more to terrestrial or shallow-marine eruptions than to eruptions in deep offshore areas. The role of hydrotherms associated with mid-ocean ridge volcanism is debatable. The contents of Os in modern MOR hydrothermal fluids approach those in seawater and cannot change its Os isotope composition (Turgeon and Creaser, 2008).

Magmatic activity coeval with the Bonarelli event lasted ca. 600 kyr, from ~350 kyr before OAE2 to ~240 kyr after its onset, as estimated from Os isotope data combined with available radioisotope ages (Du Vivier et al., 2015b). Prominent metal anomalies in WIS sections record brief but voluminous eruptions that lasted from several days to several decades (Snow et al., 2005). An especially large pulse occurred about 23 kyr before OAE2, according to Os and C isotope data (Turgeon and Creaser, 2008).

Thus, the onset of the Bonarelli event fits the best the beginning of the major magmatic event in the Caribbean Province. However, it was the time of voluminous outpourings in different provinces worldwide, while precise dating and correlation of large magmatic pulses is not always possible for data shortage. Several possibilities are: (1) eruptions in the Caribbean Plateau contributed a lot to anoxia; they increased the productivity of the North Atlantic and Tethys Oceans and extended the zone of oxygen minimum in the Pacific; (2) activity in other large igneous provinces likewise increased seawater productivity, at least on the regional scale; global magmatism reached some threshold level in the Late Cenomanian and perturbed geochemical cycles; (3) MOR hydrothermal systems may have been an additional source of biolimiting elements during periods of very fast spreading.

The isotope ages of lavas show that quite intense volcanism continued on the Earth after the end of OAE2, though the compositions of Os and other isotopes with relatively short residence times indicate decay of volcanic activity in the latest Cenomanian.

CLIMATE CHANGE DURING THE BONARELLI EVENT

The mid-Cretaceous superplume episode caused a long period of high sea stand and climate warming due to CO_2 emanation (Larson, 1991). Warming led to oxygen depletion in oceans (Huber et al., 2002) and additional CO_2 release into the air increasing the greenhouse effect (Wignall, 2001). The accelerated hydrological cycles and enhanced weathering under high p_{CO_2} on continents maintained increasing inputs of nutrients into oceans (Jenkyns, 2010; Pogge von Strandmann et al., 2013).

There is a wealth of paleontological and geochemical evidence for the mid-Cretaceous greenhouse climate, with high seawater temperatures. Sea surface temperatures from 25 °C at high latitudes to 35–36 °C at the equator were inferred from $\delta^{18}O$ values of carbonates and foraminifera, as well as from TEX_{86} (an organic paleothermometer based on the degree of cyclization on 86-carbon membrane lipids produced by mesophilic *Thaumarchaeota*) of C/T black shales (Jenkyns et al., 2004, 2007; Smyshlaeva, 2005; Zakharov et al., 2006; Forster et al., 2007). Middle bathyal waters in the latest Cenomanian were as warm as 15 to 20 °C, according to $\delta^{18}O$ data (Huber et al., 2002). Lower density gradients in the water column facilitated vertical fluxes of nutrients and thus were another factor supporting productivity (Hay, 2009; Leckie et al., 2002). The sea surface temperatures became 3–4 °C colder for 150 kyr after the positive $\delta^{13}C$ excursion, in the time of the Plenus cooling in Europe (Forster et al., 2007; Sinninghe Damsté et al., 2010; Jarvis et al., 2011). The Plenus event was attributed to accelerated C_{org} sequestration and the respective reduction of atmospheric CO_2; low p_{CO_2} was confirmed by changes in the stomatal index estimated for fossil plant cuticles (Barclay et al., 2010). Then the sea surface temperatures and atmospheric CO_2 were growing till the Early Turonian maximum which correlated with the Cretaceous highest sealevel (Kuypers et al., 1999; Huber et al., 2002; Forster et al., 2007; Jarvis et al., 2011).

Warming in the beginning of OAE2 and after the Plenus event was coeval to two pulses of volcanism marked by high contents of metals in sediments (Pearce et al., 2009). During the first pulse, CO_2 emission was balanced by C_{org} sequestration, but the amount of emitted CO_2 during the second pulse exceeded that of buried CO_2, and the Early Turonian temperature maximum postdated the end of OAE2 (Jarvis et al., 2011). Therefore, climate change hardly was the main and sufficient cause for the cessation of anoxia. Changes in nutrient fluxes and productivity of biota or ocean circulation may have played a more important part in the closing of OAE2.

EFFECT OF OCEAN CIRCULATION ON THE OAE2 EVOLUTION

Nd isotope composition is a good proxy of past ocean circulation, but the available data are insufficient to reconstruct its complete mid-Cretaceous history, while the climate and biogeochemical modeling is often ambigous. The modeling results require additional checks against lithological, geochemical, and paleontological evidence which is quite scanty for the Indian Ocean and East Tethys basins. Therefore, the consideration below is limited to Atlantic, West Tethys, and Pacific circulation.

Most models show that the mid-Cretaceous Pacific Ocean was well ventilated and oxygenated, and its wind-driven circulation had analogs of all modern currents except for the

Antarctic circumpolar current (Barron and Peterson, 1990). According to another model, seasonal winds of different directions induced mesoscale eddies and water mixing in the mid-Cretaceous time in the absence of stable winds in high and middle latitudes (Hay, 2009). Both scenarios are consistent with the lack of anoxic sediments in deep parts of the Pacific and their presence on top of rises that fell within local oxygen minimum zones. These zones formed by turbulent upwelling above the rises in the equatorial zone of divergence (Sliter and Premoli Silva, 1990; Hay, 2009, 2011). The existence of active circulation is confirmed by the scarcity of C/T boundary deposits in the Pacific because of erosion by strong currents (Basov and Vishnevskaya, 1991).

Enhanced accumulation of organic carbon in sediments of the southern NPA from the Late Aptian to the Early Turonian, with a peak during OAE2, has had several explanations. One hypothesis implies that this part of the ocean was prone to O_2 depletion in the middle Cretaceous, because it was confined between sills that reduced deep ocean ventilation; furthermore, the northern border of the area at around 50° N was too far from the pole to be a source of deep waters (Monteiro et al., 2012). Deep waters formed at that time on broad Arctic shelves open into the Pacific Ocean and in the southern Pacific (Hay, 2011; Hasegawa et al., 2013; Donnadieu et al., 2016), and they became already depleted in O_2 when reached NPA (Monteiro et al., 2012). The mid-Cretaceous ε_{Nd} increase (from –8 to –4) in the Atlantic and Indian Oceans was presumably due to weak circulation that was favorable for accumulation of radiogenic Nd carried by volcanic dust (Robinson et al., 2010). Less radiogenic ε_{Nd} values since the Campanian indicate the onset of active circulation and deep water formation in the southern Atlantic and Indian Oceans (Donnadieu et al., 2016; Robinson et al., 2010). The circulation changes may result from climate cooling, South Atlantic spreading, and deepening of the strait between the Central Atlantic and Pacific Oceans. Modeling (Poulsen et al., 2001) shows that the Antarctic bottom water began ventilating the Atlantic basin already in the Turonian. Intense circulation of deep waters apparently favored the decay of OAE2 and prevented further development of anoxia.

In the Cretaceous, bottom waters formed on a regional scale in subtropical shallow seas, at intensity proportional to the sea surface temperature and evaporation rates. Seawater was saline and warm, i.e., poor in O_2 (Poulsen et al., 2001), and thus maintained anoxia and influenced regional upwellings carrying nutrients to the surface.

According to some models, the mid-Cretaceous global thermohaline circulation was as intense as at present or slightly greater (Trabucho-Alexandre et al., 2010), with high-speed zonal winds and related upwelling (Jones and Jenkyns, 2001). The relatively intense thermohaline circulation (Trabucho-Alexandre et al., 2010), at the paleogeographic conditions and air circulation in NPA, made it a trap for nutrients since the mid-Cretaceous time. The long axis of the basin was aligned with the direction of trade winds which created a current of surface waters toward the Pacific which coexisted with a W–E flow of subsurface waters into NPA. Intermediate waters carried from the Pacific nutrients produced by submarine magmatism. Later the nutrients rose into the euphotic zone by upwelling driven by trade winds along the southern margins of the North Atlantic basin which made this region a focus of black shale deposition. Lesser amounts of nutrients could reach the Tethys and North Atlantic basins, and C_{org} burial was thus less voluminous and occurred only in the Late Cenomanian. The model is consistent with the observed spatial distribution of element anomalies at the C/T boundary (Orth et al., 1993). The high sea stand facilitated water flow through the strait and reduced clastic input into organic-rich sediments. Black shale deposition stopped in the Early Turonian when the equatorial Atlantic region became open to deep waters and the circulation changed to Pacific-ward transport of water masses at all depths (Trabucho-Alexandre et al., 2010; Donnadieu et al., 2016).

Thus, paleogeography affected largely the ocean circulation, oxygen inputs, and the distribution of nutrients, which created prerequisites for the onset or decay of anoxia.

OCEAN PRODUCTIVITY CHANGES DURING OAE2

Modeling shows that productivity, along with paleogeography, is a key control of oxygen depletion in oceans (Monteiro et al., 2012). The Bonarelli event was marked by high productivity of surface waters and changes in planktonic communities. The European sections exhibit dramatic $CaCO_3$ reduction at the OAE2 level (Schlanger et al., 1987; Kuroda et al., 2005; Turgeon and Brumsack, 2006) caused by a crisis of carbonate plankton. Among possible reasons are the acidification of water as a result of magmatism-related CO_2 emission (Erba and Bottini, 2009) and its eutrophication with the ensuing growth of organic-walled plankton at the expense of calcareous species. Pelagic black shale in the OAE2 interval in sites 144, 367 and 603B DSDP from NPA contains high percentages of 2-methylhopanoids (membrane lipids common to cyanobacteria). The isotope composition ($\delta^{15}N$) of nitrogen in sediments indicates its fixation during the deposition. Nitrogen-fixing cyanobacteria were important producers of organic carbon in sediments deposited during the Bonarelli event (Kuypers et al., 2004b). They gained advantage over algae in the conditions of nitrate reduction giving rise to denitrification and/or anaerobic ammonium oxidation leading ultimately to N_2 loss to the atmosphere and its unavailability to organisms (Jenkyns et al., 2007).

Maintaining high ocean productivity during OAE required high inputs of biologically significant elements (N, P, Fe, etc.), by several possible mechanisms (Fig. 4): (1) hydrothermal activity (Sinton and Duncan, 1997; Snow et al., 2005; MacLeod et al., 2008); (2) enhanced river-borne nutrient fluxes in a warm climate, at accelerated hydrological

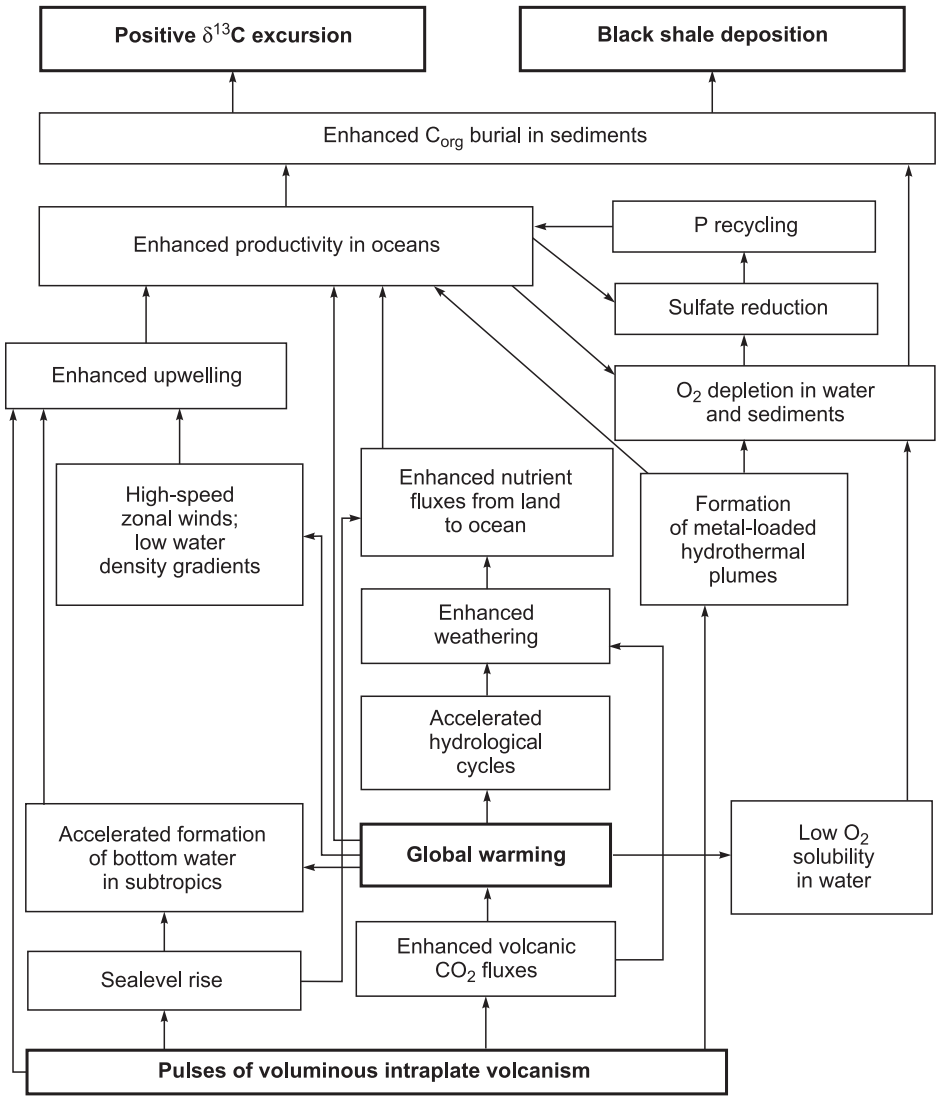

Fig. 4. Effects of volcanism on black shale deposition and $\delta^{13}C$ excursions. Compiled with reference to published data (Jones and Jenkyns, 2001; Meyer and Kump, 2008; Adams et al., 2010).

cycle and weathering (Pogge von Strandmann et al., 2013); (3) leaching of nutrients from shelf areas flooded during transgression (Gavrilov et al., 2002; Mort et al., 2008); (4) increased inputs of phosphorus from sediments due to reduction of iron oxyhydroxides that bind phosphates, along with restriction of authigenic Ca–P minerals formation in dysoxic/anoxic conditions (Van Cappellen and Ingall, 1994; Kraal et al., 2010; Poulton et al., 2015); (5) nitrogen fixation by cyanobacteria that supported their own productivity, as well as the productivity of organisms of higher trophic levels (Kuypers et al., 2004b). Supply of biolimiting elements into the photic zone of specific areas requires strong upwelling of intermediate and deep waters (Poulsen et al., 2001; Trabucho-Alexandre et al., 2010). These mechanisms could act separately or jointly in different combinations in specific areas during specific anoxic events.

In spite of its global spread, the positive $\delta^{13}C$ excursion related to OAE2 was induced by local burial of C_{org} at euxinic hotspots (Owens et al., 2013), especially in southern NPA. For instance, ~2% of excessive C_{org} buried during OAE2 was deposited in a single basin of Tarfaya over an area as small as 0.05% of the Earth's C/T seafloor (Kolonic et al., 2005). Seawater Mo depletion in such basins limited the availability of nitrogenase, a complex of Mo-bearing enzymes required for nitrogen fixation by cyanobacteria (Owens et al., 2016), and thus reduced the productivity.

Variations throughout the section in P accumulation rates ($mg/cm^2/kyr$), hydrogen index (HI), and C/P ratios can be used to reconstruct the history of the Bonarelli event. Accumulation of phosphorus was fast in the beginning of OAE2, then slowed down till the end of the event, and then accelerated again. This trend was observed in sections of the Demerara Rise, Tarfaya basin, Central Italy, South Spain, southern England, WIS, and Tibet (Mort et al., 2007b, 2008; Kraal et al., 2010; Bomou et al., 2013). High concentrations and accumulation rates of P early during OAE2, immedi-

ately before and in the beginning of the $\delta^{13}C$ excursion, record productivity increase (mechanisms 1, 2, and 3 listed above). Organic carbon was poorly preserved at that time (low HI), and its oxidation liberated phosphorus which formed authigenic minerals. In the major OAE2 phase, phosphorus was lost from sediments (increasing C/P ratios) and then became again involved in the turnover and maintained high productivity. Later during OAE2, the productivity reduced while C_{org} accumulated mainly due to its preservation in the conditions of oxygen depletion (Mort et al., 2007a). After OAE2, the burial of P was more effective than that of C_{org} and the C/P ratios in sediments decreased correspondingly.

High productivity during the Bonarelli event led to (i) carbon sequestration in sediments; (ii) O_2 increase by atmospheric and oceanic photosynthesis and the ensuing P flux into sediments, as well as more effective oxidation of organic carbon (Kuypers et al., 2004b; Mort et al., 2007a); (iii) large-scale sulfate reduction which decreased the oceanic SO_4^{2-} sink and increased the O_2 flux into the atmosphere (Ohkouchi et al., 1999); as a consequence, sulfate reduction slowed down and phosphorus again became bound in Fe oxyhydrates (Adams et al., 2010); (iv) inputs of biologically significant elements into sediments and their removal from water which limited the productivity (Owens et al., 2013, 2016). All these processes, together with changes in ocean circulation and possible decay of volcanism, ultimately led OAE2 to the end, and the ocean returned to more oxic conditions.

CONCLUSIONS

The Bonarelli event was the largest Cretaceous anoxic event that lasted ca. 600 kyr. Studies of its imprints in sediments provide clues to many sedimentary, biotic, and geochemical processes that occurred near the Cenomanian–Turonian (C/T) boundary, and to their relationships. Black shale deposition of that time was maintained by favorable paleogeographic conditions and ocean circulation, and nutrient inputs into oceans. The event had a global extent, though the deposition of organic-rich sediments was not quite synchronous globally and became unevenly distributed. Most of black shale deposition occurred in the Northern Proto-Atlantic region, while in the Pacific, carbonaceous sediments formed on a much smaller scale and only in the equatorial part.

The distribution of metal anomalies and stable isotope ratios record enhanced volcanic and hydrothermal activity in the latest Cenomanian, including two large magmatic pulses: immediately before OAE2 and in the beginning of the $\delta^{13}C$ plateau. These pulses correlate with increase in atmospheric CO_2 and temperature inferred from independent data. Some isotope shifts may be evidence of enhanced continental weathering in the beginning of OAE2, apparently related to CO_2 emission into the atmosphere during voluminous volcanic eruptions and climate warming.

The Bonarelli event correlates with some isotope ages of volcanism from different large igneous provinces: a major pulse of continental flood basalt volcanism in the Caribbean immediately before OAE2; latest Cenomanian volcanism in the Arctic province, on the Kerguelen and Ontong Java Plateaus, in the Broken Ridge, and on volcanic rises in the western Pacific.

Voluminous lava outpourings triggered some processes that led to greater availability of nutrients and stimulated surface water productivity in oceans. As a result, much oxygen became consumed by decomposition of organic carbon, and the anoxic and euxinic conditions spread over large oceanic areas. During the major OAE2 phase, productivity was also maintained by recycling of P from dysoxic/anoxic sediments. The chart of main processes and mechanisms triggering and maintaining anoxia (Fig. 4) is workable for a greenhouse climate with poor seawater stratification. Zones of weak deep water circulation in the narrow basin of the opening Atlantic Ocean became traps for nutrients, which was an important factor of anoxia.

Some geochemical and biochemical processes associated with high productivity ultimately led to its decrease. This is a bright illustration of the biosphere ability to recover the environment by overcoming the perturbations to geochemical cycles. In the course of the Bonarelli event, toxic and biologically significant elements were sequestered in sediments while the productivity reduction was favorable for the return to oxic conditions in oceans. The atmospheric pressure p_{CO_2} and the temperature remained high in the end of OAE2, which may be evidence of further volcanic CO_2 inputs. As the volcanism abated, atmospheric carbon dioxide escaped to organic-rich sediments that were depositing in the southern NPA region for a while after the end of OAE2, as well as into carbonates in epicontinental seas. Increased Atlantic oceanic water circulation likewise favored the cessation of anoxia.

The study was supported by grant 16-05-00546 from the Russian Foundation for Basic Research.

REFERENCES

Adams, D.D., Hurtgen, M.T., Sageman, B.B., 2010. Volcanic triggering of a biogeochemical cascade during Oceanic Anoxic Event 2. Nature Geosci. 3, 201–204.

Ando, A., Nakano, T., Kaiho, K., Kobayashi, T., Kokado, E., Khim, B.-K., 2009. Onset of seawater $^{87}Sr/^{86}Sr$ excursion prior to Cenomanian–Turonian Oceanic Anoxic Event 2? New Late Cretaceous strontium isotope curve from the central Pacific Ocean. J. Foraminiferal Res. 39 (4), 322–334.

Arthur, M.A., Dean, W.E., Pratt, L.M., 1988. Geochemical and climatic effects of increased marine organic carbon burial at the Cenomanian/Turonian boundary. Nature 335, 714–717.

Barclay, R.S., McElwain, J.C., Sageman, B.B., 2010. Volcanic CO_2 pulse activates carbon sequestration during Cretaceous Oceanic Anoxic Event 2. Nature Geosci. 3, 205–208.

Barron, E.J., Peterson, W.H., 1990. Mid-Cretaceous ocean circulation: results from model sensitivity studies. Paleoceanography 5 (3), 319–337.

Basov, I.A., Vishnevskaya, V.S., 1991. Upper Mesozoic Stratigraphy of the Pacific Ocean [in Russian]. Nauka, Moscow.

Blättler, C.L., Jenkyns, H.C., Reynard, L.M., Henderson, G.M., 2011. Significant increases in global weathering during Oceanic Anoxic Events 1a and 2 indicated by calcium isotopes. Earth Planet. Sci. Lett. 309 (1–2), 77–88.

Bomou, B., Adatte, T., Tantawy, A.A., Mort, H., Fleitmann, D., Huang, Y., Föllmi, K.B., 2013. The expression of the Cenomanian–Turonian oceanic anoxic event in Tibet. Palaeogeogr. Palaeoclimatol. Palaeoecol. 369, 466–481.

Bralower, T.J., 2008. Volcanic cause of catastrophe. Nature 454 (7202), 285–287.

Bralower, T.J., Fullagar, P.D., Paull, C.K., Dwyer, G.S., Leckie, R.M., 1997. Mid-Cretaceous strontium-isotope stratigraphy of deep-sea sections. Geol. Soc. Am. Bull. 109, 1421–1442.

Broecker, W., Peng, T., 1982. Tracers in the Sea. Eldigio Press, Lamont-Doherty Geological Observatory, Palisades, New York.

Coccioni, R., Galeotti, S., 2003. The mid-Cenomanian Event: prelude to OAE2. Palaeogeogr. Palaeoclimatol. Palaeoecol. 190, 427–440.

Dean, W.E., Claypool, G.E., Thiede, J., 1981. Origin of organic-carbon-rich mid-Cretaceous limestones, Mid-Pacific Mountains and Southern Hess Rise, in: Initial Reports of the Deep Sea Drilling Project. Washington, Vol. 62, pp. 877–890.

Dickson, A.J., Jenkyns, H.C., Porcelli, D., van den Boorn, S., Idiz, E., 2016. Basin-scale controls on the molybdenum-isotope composition of seawater during Oceanic Anoxic Event 2 (Late Cretaceous). Geochim. Cosmochim. Acta 178, 291–306.

Donnadieu, Y., Pucéat, E., Moiroud, M., Guillocheau, F., Deconinck, J.-F., 2016. A better-ventilated ocean triggered by Late Cretaceous changes in continental configuration. Nature Commun. 7, 10316. DOI:10.1038/ncomms10316.

Du Vivier, A.D.C., Selby, D., Sageman, B.B., Jarvis, I., Gröcke, D.R., Voigt, S., 2014. Marine $^{187}Os/^{188}Os$ isotope stratigraphy reveals the interaction of volcanism and ocean circulation during Oceanic Anoxic Event 2. Earth Planet. Sci. Lett. 389, 23–33.

Du Vivier, A.D.C., Jacobson, A.D., Lehn, G.O., Selby, D., Hurtgen, M.T., Sageman, B.B., 2015a. Ca isotope stratigraphy across the Cenomanian–Turonian OAE2: Links between volcanism, seawater geochemistry, and the carbonate fractionation factor. Earth Planet. Sci. Lett. 416, 121–131.

Du Vivier, A.D.C., Selby, D., Condon, D.J., Takashima, R., Nishi, H., 2015b. Pacific $^{187}Os/^{188}Os$ isotope chemistry and U–Pb geochronology: Synchroneity of global Os isotope change across OAE2. Earth Planet. Sci. Lett. 428, 204–216.

Eldrett, J.S., Minisini, D., Bergman, S.C., 2014. Decoupling of the carbon cycle during ocean anoxic event 2. Geology 42, 567–570.

El-Sabbagh, A., Tantawy, A.A., Keller, G., Khozyem, H., Spangenberg, J., Adatte, T., Gertsch, B., 2011. Stratigraphy of the Cenomanian–Turonian Oceanic Anoxic Event OAE2 in shallow shelf sequences of NE Egypt. Cretaceous Res. 32, 705–722.

Erba, E., Bottini, C., 2009. The response of Cretaceous calcareous nannoplankton to pCO_2 and ocean acidification. Geochim. Cosmochim. Acta 73 (13S), A334.

Forster, A., Schouten, S., Moriya, K., Wilson, P.A., Sinninghe Damsté, J.S., 2007. Tropical warming and intermittent cooling during the Cenomanian/Turonian oceanic anoxic event 2: Sea surface temperature records from the equatorial Atlantic. Paleoceanography 22, PA1219.

Forster, A., Kuypers, M.M.M., Turgeon, S.C., Brumsack, H.-J., Petrizzo, M.R., Sinninghe Damsté, J.S., 2008. The Cenomanian/Turonian oceanic anoxic event in the South Atlantic: New insights from a geochemical study of DSDP Site 530A. Palaeogeogr. Palaeoclimatol. Palaeoecol. 267, 256–283.

Frey, F.A., Coffin, M.F., Wallace, P.J., Weis, D., 2003. Leg 183 synthesis: Kerguelen Plateau–Broken Ridge—a large igneous province, in: Proceedings of the Ocean Drilling Program, Scientific Results. College Station, Texas, Vol. 183, pp. 1–48.

Frijia, G., Parente, M., 2008. Strontium isotope stratigraphy in the upper Cenomanian shallow-water carbonates of the southern Apennines: Short-term perturbations of marine $^{87}Sr/^{86}Sr$ during the oceanic anoxic event 2. Palaeogeogr. Palaeoclimatol. Palaeoecol. 261, 15–29.

Gavrilov, Yu.O., Shchepetova, E.V., Baraboshkin, E.Yu., Shcherbinina, E.A., 2002. An Early Cretaceous anoxic basin of the Russian plate: sedimentology and geochemistry. Litologiya i Poleznye Iskopaemye, No. 4, 359–380.

Gavrilov, Yu.O., Shcherbinina, E.A., Golovanova, O.V., Pokrovskii, B.G., 2013. The Late Cenomanian paleoenvironmental event OAE2 in the East Caucasian basin of Northern Perithethys. Litologiya i Poleznye Iskopaemye, No. 6, 522–551.

Hasegawa, T., 2003. Cretaceous terrestrial paleoenvironments of northeastern Asia suggested from carbon isotope stratigraphy: Increased atmospheric pCO_2-induced climate. J. Asian Earth Sci. 21, 849–859.

Hasegawa, T., Crampton, J.S., Schiøler, P., Field, B., Fukushi, K., Kakizaki, Y., 2013. Carbon isotope stratigraphy and depositional oxia through Cenomanian/Turonian boundary sequences (Upper Cretaceous) in New Zealand. Cretaceous Res. 40, 61–80.

Hauff, F., Hoernle, K., van den Bogaard, P., Alvarado, G.E., Garbe-Schonberg, C.D., 2000. Age and geochemistry of basaltic complexes in western Costa Rica: Contributions to the geotectonic evolution of Central America. Geochem. Geophys. Geosyst. 1 (5). DOI: 10.1029/1999GC000020.

Hay, W.W., 2009. Cretaceous oceans and ocean modelling, in: Hu, X., Wang, Ch., Scott R.W., Wagreich, M., Jansa, L. (Eds.), Cretaceous Oceanic Red Beds. Stratigraphy, Composition, Origins, Paleoceanographic and Paleoclimatic Significance. SEPM Spec. Publ. 91, pp. 243–271.

Hay, W.W., 2011. Can humans force a return to a 'Cretaceous' climate? Sediment. Geol. 235, 5–26.

Herrle, J.O., Schröder-Adams, C.J., Davis, W., Pugh, A.T., Galloway, J.M., Fath, J., 2015. Mid-Cretaceous High Arctic stratigraphy, climate, and oceanic anoxic events. Geology 43 (5), 403–406.

Hetzel, A., Böttcher, M.E., Wortmann, U.G., Brumsack, H., 2009. Paleo-redox conditions during OAE2 reflected in Demerara Rise sediment geochemistry (ODP Leg 207). Palaeogeogr. Palaeoclimatol. Palaeoecol. 273, 302–328.

Hoernle, K., Hauff, F., van den Bogaard, P., 2004. 70 m.y. history (139–69 Ma) for the Caribbean large igneous province. Geology 32 (8), 697–700.

Holbourn, A., Kuhnt, W., 2002. Cenomanian–Turonian palaeoceanographic change on the Kerguelen Plateau: A comparison with Northern Hemisphere records. Cretaceous Res. 23, 333–349.

Holmden, C., Jacobson, A.D., Sageman, B.B., Hurtgen, M.T., 2016. Response of the Cr isotope proxy to Cretaceous Ocean Anoxic Event 2 in a pelagic carbonate succession from the Western Interior Seaway. Geochim. Cosmochim. Acta 186, 277–295.

Huber, B.T., Norris, R.D., MacLeod, K.G., 2002. Deep-sea paleotemperature record of extreme warmth during the Cretaceous. Geology 30 (2), 123–126.

Jarvis, I., Gale, A.S., Jenkyns, H.C., Pearce, M.A., 2006. Secular variation in Late Cretaceous carbon isotopes: A new $\delta^{13}C$ carbonate reference curve for the Cenomanian–Campanian (99.6–70.6 Ma). Geol. Mag. 143, 561–608.

Jarvis, I., Lignum, J.S., Gröcke, D.R., Jenkyns, H.C., Pearce, M.A., 2011. Black shale deposition, atmospheric CO_2 drawdown, and cooling during the Cenomanian–Turonian ocean anoxic event. Paleoceanography 26, PA3201.

Jenkyns, H.C., 2010. Geochemistry of oceanic anoxic events. Geochem. Geophys. Geosyst. 11 (3), Q03004.

Jenkyns, H.C., Gale, A.S., Corfield, R.M., 1994. Carbon- and oxygen-isotope stratigraphy of the English Chalk and Italian Scaglia and its palaeoclimatic significance. Geol. Mag. 131, 1–34.

Jenkyns, H.C., Mutterlose, J., Sliter, W.V., 1995. Upper Cretaceous carbon- and oxygen-isotope stratigraphy of deep-water sediments from the North-Central Pacific (Site 869, flank of Pikinni-Wodejebato, Marshall Islands), in: Proceedings of the Ocean Drilling Program, Scientific Results. College Station, Texas, Vol. 143, pp. 105–110.

Jenkyns, H.C., Forster, A., Schouten, S., Sinninghe Damsté, J.S., 2004. High temperatures in the Late Cretaceous Arctic Ocean. Nature 432, 888–892.

Jenkyns, H.C., Matthews, A., Tsikos, H., Erel, Y., 2007. Nitrate reduction, sulfate reduction, and sedimentary iron isotope evolution during the Cenomanian–Turonian oceanic anoxic event. Paleoceanography 22, PA3208.

Jones, C.E., Jenkyns, H.C., 2001. Seawater strontium isotopes, oceanic anoxic events, and seafloor hydrothermal activity in the Jurassic and Cretaceous. Am. J. Sci. 301, 112–149.

Karakitsios, V., Tsikos, H., van Breugel, Y., Koletti, L., Sinninghe Damsté, J.S., Jenkyns, H.C., 2007. First evidence for the Cenomanian–Turonian oceanic anoxic event (OAE2, 'Bonarelli' event) from the Ionian Zone, western continental Greece. Int. J. Earth Sci. 96 (2), 343–352.

Kolonic, S., Wagner, T., Forster, A., Sinninghe Damsté, J.S., Walsworth-Bell, B., Erba, E., Turgeon, S., Brumsack, H.-J., Chellai, E.H., Tsikos, H., Kuhnt, W., Kuypers, M.M.M., 2005. Black shale deposition on the northwest African Shelf during the Cenomanian/Turonian oceanic anoxic event: Climate coupling and global organic carbon burial. Paleoceanography 20, 95–128.

Kraal, P., Slomp, C.P., Forster, A., Kuypers, M.M.M., 2010. Phosphorus cycling from the margin to abyssal depths in the proto-Atlantic during oceanic anoxic event 2. Palaeogeogr. Palaeoclimatol. Palaeoecol. 295, 42–54.

Kuroda, J., Ohkouchi, N., 2006. Implication of spatiotemporal distribution of black shales deposited during the Cretaceous oceanic anoxic event-2. Paleontol. Res. 10 (4), 345–358.

Kuroda, J., Ohkouchi, N., Ishii, T., Tokuyama, H., Taira, A., 2005. Lamina-scale analysis of sedimentary components in Cretaceous black shales: Paleoceanographic implications for oceanic anoxic events. Geochim. Cosmochim. Acta 69, 1479–1494.

Kuroda, J., Ogawa, N.O., Tanimizu, M., Coffin, M.F., Tokuyama, H., Kitazato, H., Ohkouchi, N., 2007. Contemporaneous massive subaerial volcanism and late cretaceous Oceanic Anoxic Event 2. Earth Planet. Sci. Lett. 256, 211–223.

Kuypers, M.M.M., Pancost, R.D., Sinninghe Damsté, J.S., 1999. A large and abrupt fall in atmospheric CO_2 concentration during Cretaceous times. Nature 399, 342–345.

Kuypers, M.M.M., Pancost, R.D., Nijenhuis, I.A., Sinninghe Damsté, J.S., 2002. Enhanced productivity led to increased organic carbon burial in the euxinic North Atlantic basin during the late Cenomanian oceanic anoxic event. Paleoceanography 17 (4), PA1051.

Kuypers, M.M.M., Lourens, L.J., Rijpstra, W.I.C, Pancost, R.D., Nijenhuis, I.A., Sinninghe Damsté, J.S., 2004a. Orbital forcing of organic carbon burial in the proto-North Atlantic during oceanic anoxic event 2. Earth Planet. Sci. Lett. 228, 465–482.

Kuypers, M.M.M., van Breugel, Y., Schouten, S., Erba, E., Sinninghe Damsté, J.S., 2004b. N_2-fixing cyanobacteria supplied nutrient N for Cretaceous oceanic anoxic events. Geology 32 (10), 853–856.

Larson, R.L., 1991. Geological consequences of superplumes. Geology 19, 963–966.

Lebedeva, N.K., Zverev, K.V., 2003. Sedimentological and palynological analysis of the Cenomanian–Turonian event in northern Siberia. Geologiya i Geofizika (Russian Geology and Geophysics) 44 (8), 769–780 (739–749).

Leckie, R.M., Bralower, T.J., Cashman R., 2002. Oceanic anoxic events and plankton evolution: Biotic response to tectonic forcing during the mid-Cretaceous. Paleoceanography 17 (3), 13-1–13-29. DOI: 10.1029/2001PA000623.

Lenniger, M., Nøhr-Hansen, H., Hills, L.V., Bjerrum, C.J., 2014. Arctic black shale formation during Cretaceous Oceanic Anoxic Event 2. Geology 42 (9), 799–802.

Levitan, M.A., Alekseev, A.S., Badulina, N.V., Girin, Yu.P., Kopaevich, L.F., Kubrakova, I.V., Tyutyunnik, O.A., Chudetskii, M.Yu., 2010. Geochemistry of sediments at the Cenomanian-Turonian boundary in Mountainous Crimea and Northwestern Caucasus. Geokhimiya 6, 570–591.

Li, G., Jiang, G., Hu, X., Wan, X., 2009. New biostratigraphic data from the Cretaceous Bolinxiala Formation in Zanda, southwestern Tibet of China, and their paleogeographic and paleoceanographic implications. Cretaceous Res. 30, 1005–1018.

Luciani, V., Cobianchi, M., 1999. The Bonarelli Level and other black shales in the Cenomanian-Turonian of the northeastern Dolomites (Italy): Calcareous nannofossil and foraminiferal data. Cretaceous Res. 20, 135–167.

MacLeod, K.G., Martin, E.E., Blair, S.W., 2008. Nd isotopic excursion across Cretaceous ocean anoxic event 2 (Cenomanian-Turonian) in the tropical North Atlantic. Geology 36, 811–814.

Magtoto, C.Y., Fernando, A.G.S., Takashima, R., Nishi, H., Tomosugi, T., 2014. Calcareous nannofossil biostratigraphy of the Cenomanian–Turonian oceanic anoxic event 2 (OAE2) record in California, USA, in: Proc. 2nd Int. Symp. International Geoscience Programme (IGCP), Project 608 "Cretaceous Ecosystems and Their Responses to Paleoenvironmental Changes in Asia and the Western Pacific", Abstract Volume. Tokyo, p. 32.

Mahoney, J.J., Storey, M., Duncan, R.A., Spencer, K.J., Pringle, M., 1993. Geochemistry and geochronology of Leg 130 basement lavas: nature and origin of the Ontong Java plateau, in: Proceedings of the Ocean Drilling Program, Scientific Results. College Station, Texas, Vol. 130, pp. 3–22.

Mahoney, J.J., Fitton, J.G., Wallace, P.J., Antretter, M.J., Banerjee, N.R., Bergen, J.A., Cairns, G., Castillo, P.R., Chambers, L.M., Chazey III, W.J., Coffin, M.F., Godard, M.M., Hall, S.A., Honnorez, J., Ingle, S.P., Kroenke, L.W., MacLeod, K.G., Naruse, H., Neal, C.R., Ogg, J.G., Riisager, P., Sano, T., Sikora, P.J., van der Werff, W., White, R.V., Zhao, X., 2001. Leg 192 Summary, in: Proceedings of the Ocean Drilling Program, Initial Reports. College Station, Texas, Vol. 192, pp. 1–75.

Martin, E.E., MacLeod, K.G., Jimenez, Berrocso, A., Bourbon, E., 2012. Water mass circulation on Demerara Rise during the Late Cretaceous based on Nd isotopes. Earth Planet. Sci. Lett. 327–328, 111–120.

McArthur, J.M., Howarth, R.J., Shields, G.A., 2012. Strontium isotope stratigraphy, in: The Geologic Time Scale. Elsevier, Amsterdam, pp. 127–144.

Meyer, K.M., Kump, L.R., 2008. Oceanic euxinia in Earth history: Causes and consequences. Ann. Rev. Earth Planet. Sci. 36, 251–288.

Meyers, S.R., Siewert, S.E., Singer, B.S., Sageman, B.B., Condon, D.J., Obradovich, J.D., Jicha, B.R., Sawyer, D.A., 2012. Intercalibration of radioisotopic and astrochronologic time scales for the Cenomanian–Turonian boundary interval, Western Interior Basin, USA. Geology 40, 7–10.

Moiroud, M., Pucéat, E., Donnadieu, Y., Bayon, G., Moriya, K., Deconinck, J.-F., Boyet, M., 2013. Evolution of the neodymium isotopic signature of neritic seawater on a northwestern Pacific margin: new constrains on possible end-members for the composition of deep-water masses in the Late Cretaceous ocean. Chem. Geol. 356, 160–170.

Monteiro, F.M., Pancost, R.D., Ridgwell, A., Donnadieu, Y., 2012. Nutrients as the dominant control on the spread of anoxia and euxinia across the Cenomanian-Turonian oceanic anoxic event (OAE2): Model-data comparison. Paleoceanography 27, PA4209.

Montoya-Pino, C., Weyer, S., Anbar, A.D., Pross, J., Oschmann, W., van de Schootbrugge, B., Arz, H.W., 2010. Global enhancement of ocean anoxia during Oceanic Anoxic Event 2: a quantitative approach using U isotopes. Geology 38, 315–318.

Mort, H.P., Adatte, T., Föllmi, K.B., Keller, G., Steinmann, P., Matera, V., Berner, Z., Stüben, D., 2007a. Phosphorus and the roles of

productivity and nutrient recycling during oceanic anoxic event 2. Geology 35 (6), 483–486.

Mort, H., Jacquat, O., Adatte, T., Steinmann, P., Föllmi, K.B., Matera, V., Berner, Z., Stüben. D., 2007b. The Cenomanian/Turonian anoxic event at the Bonarelli Level in Italy and Spain: enhanced productivity and/or better preservation? Cretaceous Res. 28, 597–612.

Mort, H.P., Adatte, T., Keller, G., Bartels, D., Föllmi, K.B., Steinmann, P., Berner, Z., Chellai, E.H., 2008. Organic carbon deposition and phosphorus accumulation during Oceanic Anoxic Event 2 in Tarfaya, Morocco. Cretaceous Res. 29, 1008–1023.

Naidin, D.P., 1993. Late Cretaceous events in the eastern paleobiogeographical area. Paper 2. Events at the Cenomanian-Turonian and Maastrachtian/Danian boundaries. Bull. MOIP, Ser. Geol. 68 (3), 33–53.

Nakanishi, M., Nakamura, Y., Coffin, M.F., Hoernle, K., Werner, R., 2015. Topographic expression of the Danger Islands Troughs and implications for the tectonic evolution of the Manihiki Plateau, western equatorial Pacific Ocean, in: The Origin, Evolution, and Environmental Evolution of Oceanic Large Igneous Provinces. Geol. Soc. Am., Spec. Pap. 511, pp. 195–220.

Navarro-Ramirez, J.P., Bodin, S., Immenhauser, A., 2016. Ongoing Cenomanian-Turonian heterozoan carbonate production in the neritic settings of Peru. Sediment. Geol. 331, 78–93.

Nemoto, T., Hasegawa, T., 2011. Submillennial resolution carbon isotope stratigraphy across the Oceanic Anoxic Event 2 horizon in the Tappu section, Hokkaido, Japan. Palaeogeogr. Palaeoclimatol. Palaeoecol. 309, 271–280.

Núñez-Useche, F., Canet, C., Barragán, R., Alfonso, P., 2016. Bioevents and redox conditions around the Cenomanian–Turonian anoxic event in Central Mexico. Palaeogeogr. Palaeoclimatol. Palaeoecol. 449, 205–226.

Ohkouchi, N., Kawamura, K., Kajiwara, Y., Wada, E., Okada, M., Kanamatsu, T., Taira, A., 1999. Sulfur isotope records around Livello Bonarelli (northern Apennines, Italy) black shale at the Cenomanian–Turonian boundary. Geology 27, 535–538.

Orth, C.J., Attrep, M., Quintana, L.R., Elder, W.P., Kauffman, E.G., Diner, R., Villamil, T., 1993. Elemental abundance anomalies in the late Cenomanian extinction interval: a search for the source(s). Earth Planet. Sci. Lett. 117 (1–2), 189–204.

Owens, J.D., Lyons, T.W., Li, X., Macleod, K.G., Gordon, G., Kuypers, M.M.M., Anbar, A., Kuhnt, W., Severmann, S., 2012. Iron isotope and trace metal records of iron cycling in the proto-North Atlantic during the Cenomanian–Turonian oceanic anoxic event (OAE-2). Paleoceanography 27 (3), PA3223.

Owens, J.D., Gill, B.C., Jenkyns, H.C., Bates, S.M., Severmann, S., Kuypers, M.M.M., Woodfine, R.G., Lyons, T.W., 2013. Sulfur isotopes track the global extent and dynamics of euxinia during Cretaceous oceanic anoxic event. PNAS 110 (46), 18,407–18,412.

Owens, J.D., Reinhard, C.T., Rohrssen, M., Loveb, G.D., Lyons, T.W., 2016. Empirical links between trace metal cycling and marine microbial ecology during a large perturbation to Earth's carbon cycle. Earth Planet. Sci. Lett. 449, 407–417.

Pearce, M.A., Jarvis, I., Tocher, B.A., 2009. The Cenomanian–Turonian boundary event, OAE2 and palaeoenvironmental change in epicontinental seas: New insights from the dinocyst and geochemical records. Palaeogeogr. Palaeoclimatol. Palaeoecol. 280, 207–234.

Pogge von Strandmann, P.A.P., Jenkyns, H.C., Woodfine, R.G., 2013. Lithium isotope evidence for enhanced weathering during oceanic anoxic event 2. Nature Geosci. 6, 668–672.

Portnyagin, M., Savelyev, D., Hoernle, K., Hauff, F., Garbe-Schönberg, D., 2008. Mid-Cretaceous Hawaiian tholeiites preserved in Kamchatka. Geology 36, 903–906.

Poulsen, C.J., Barron, E.J., Arthur, M.A., Peterson, W.H., 2001. Response of the mid-Cretaceous global ocean circulation to tectonic and CO_2 forcings. Paleoceanography 16 (6), 576–592.

Poulton, S.W., Henkel, S., März, C., Urquhart, H., Flögel, S., Kasten, S., Sinninghe Damsté, J.S., Wagner, T., 2015. A continental-weathering control on orbitally driven redox-nutrient cycling during Cretaceous oceanic anoxic event 2. Geology 43 (11), 963–966.

Premoli Silva, I., Haggerty, J., Rack, F., Arnaud-Vanneau, A., Bergersen, D.D., Bogdanov, Y., Bohrmann, H.W., Buchardt, B., Camoin, G., Christie, D.M., Dieu, J.J., enos, P., Erba, E., Fenner, J.M., Gee, J.S., Head, M.J., Ito, H., Hobbs, P.R.N., Jansa, L.F., Ladd, J.W., Larson, R.L., Lincoln, J.M., Hakanishi, M., Ogg, J.G., Opdyke, B.N., Pearson, P.N., Quinn, T.M., Watkins, D.K., Wilson, P.A.,, 1993. Site 872, in: Proceedings of the Ocean Drilling Program, Initial Reports. College Station, Texas, Vol. 144, pp. 105–144.

Price, G.D., 2003. New constraints upon isotope variation during the early Cretaceous (Barremian–Cenomanian) from the Pacific Ocean. Geol. Mag. 140 (5), 513–522.

Pucéat, E., 2008. A new breath of life for anoxia. Geology 36, 831–832.

Robinson, S.A., Murphy, D.P., Vance, D., Thomas, D.J., 2010. Formation of "southern component water" in the Late Cretaceous: Evidence from Nd-isotopes. Geology 38 (10), 871–874.

Sageman, B.B., Meyers, S.R., Arthur, M.A., 2006. Orbital time scale and new C-isotope record for Cenomanian–Turonian boundary stratotype. Geology 34 (2), 125–128.

Sageman, B.B., Rich, J., Arthur, M.A., Birchfield, G.E., Dean, W.E., 1997. Evidence for Milankovitch periodicities in Cenomanian–Turonian lithologic and geochemical cycles, Western Interior U.S. J. Sediment. Res. 67, 286–301.

Savelyev, D.P., 2004. Cretaceous within-plate volcanism in Eastern Kamchatka: Geological setting and effect on island arc volcanism. Geologiya i Razvedka, No. 2, 16–19.

Savelyev, D.P., Lander, A.V., Pronina, N.V., Savelyeva, O.L., 2007. The first finding of carbonaceous rocks in Cretaceous paleooceanic complexes in Eastern Kamchatka. Vestnik KRAUNTs. Ser. Nauki o Zemle 10 (2), 102–104.

Savelyev, D.P., Savelyeva, O.L., Palechek, T.N., Pokrovsky, B.G., 2012. Carbon isotope curve and iridium anomaly in the Albian-Cenomanian paleoceanic deposits of the Eastern Kamchatka, in: Geophys. Res. Abstracts, EGU General Assembly (22–27 April 2012, Vienna), Vol. 14, p. 1940.

Savelyeva, O.L., 2009. Rhythmic Sedimentation and Footprints of Anoxic Events in Cretaceous (Albian-Cenomanian) Deposits in Eastern Kamchatka. PhD Thesis [in Russian]. Moscow.

Savelyeva, O., Palechek, T., Savelyev, D., 2010. First evidence of the oceanic anoxic events in Cenomanian paleoceanic deposits of the Eastern Kamchatka. Geophys. Res. Abstracts. V. 12. EGU2010-3782, EGU General Assembly 2010.

Savelyeva, O., Palesskiy, S., Savelyev, D., 2015. PGE in Carbonaceous beds in the Cretaceous carbonate-siliceous section of the Kamchatsky Mys Peninsula (Russia), in: Goldschmidt Abstracts, p. 2779.

Schlanger, S.O., Jenkyns, H.C., 1976. Cretaceous oceanic anoxic events: Causes and consequences. Geologie en Mijnbouw 55, 179–184.

Schlanger, S.O., Arthur, M.A., Jenkyns, H.C., Scholle, P.A., 1987. The Cenomanian–Turonian oceanic anoxic event, I. Stratigraphy and distribution of organic carbon-rich beds and the marine $\delta^{13}C$ excursion, in: Marine Petroleum Source Rocks. Geol. Soc. Spec. Publ. 26, pp. 371–399.

Scopelliti, G., Bellanca, A., Coccioni, R., Luciani, V., Neri, R., Baudin, F., Chiari, M., Marcucci, M., 2004. High-resolution geochemical and biotic records of the Tethyan 'Bonarelli Level' (OAE2, latest Cenomanian) from the Calabianca–Guidaloca composite section, northwestern Sicily, Italy. Palaeogeogr. Palaeoclimatol. Palaeoecol. 208, 293–317.

Scotese, C.R., 2004. A continental drift flipbook. J. Geol. 112, 729–741.

Sedov, A.P., Matveenkov, V.V., Volokitina, L.P., Rashidov, V.A., Kazakevich, V.I., Lukiyanov, S.V., 2005. Formation of seamounts: A qualitative model. Vestnik KRAUNTs. Ser. Nauki o Zemle 5, 24–44.

Sinninghe Damsté, J.S., Köster, J., 1998. A euxinic southern North Atlantic Ocean during the Cenomanian/Turonian oceanic anoxic event. Earth Planet. Sci. Lett. 158, 165–173.

Sinninghe Damsté, J.S., Kuypers, M.M.M., Pancost, R.D., Schouten, S., 2008. The carbon isotopic response of algae, (cyano)bacteria, archaea and higher plants to the late Cenomanian perturbation of the global carbon cycle: Insights from biomarkers in black shales from the Cape Verde Basin (DSDP Site 367). Organic Geochem. 39, 1703–1718.

Sinninghe Damsté, J.S., van Bentum, E.C., Reichart, G.-J., Pross, J., Schouten, S., 2010. A CO_2 decrease-driven cooling and increased latitudinal temperature gradient during the mid-Cretaceous oceanic anoxic event 2. Earth Planet. Sci. Lett. 293, 97–103.

Sinton, C.W., Duncan, R.A., 1997. Potential links between ocean plateau volcanism and global ocean anoxia at the Cenomanian–Turonian boundary. Econ. Geol. 92, 836–842.

Sliter, W.V., Premoli Silva, I., 1990. Age and origin of Cretaceous planktonic foraminifers from limestone of the Franciscan complex near Laytonville, California. Paleoceanography 5, 639–667.

Smyshlyaeva, O.P., 2005. The Stable Isotope Composition of Cretaceous Organic Carbonates of the Russian Far East (Penzhina Guba, Crillon, Hokkaido) and Global Correlation of Late Mesozoic Events from Isotope Data. PhD Thesis [in Russian]. Vladivostok.

Snow, L.J., Duncan, R.A., Bralower, T.J., 2005. Trace element abundances in the Rock Canyon Anticline, Pueblo, Colorado, marine sedimentary section and their relationship to Caribbean plateau construction and ocean anoxic event 2. Paleoceanography 20 (3), PA3005.

Storey, M., Mahoney, J.J., Saunders, A.D., Duncan, R.A., Kelley, S.P., Coffin, M.F., 1995. Timing of hot spot-related volcanism and the breakup of Madagascar and India. Science 267 (5199), 852–855.

Takashima, R., Kawabe, F., Nishi, H., Moriya, K., Wani, R., Ando, H., 2004. Geology and stratigraphy of forearc basin sediments in Hokkaido, Japan: Cretaceous environmental events on the north-west Pacific margin. Cretaceous Res. 25, 365–390.

Takashima, R., Nishi, H., Huber, B.T., Leckie, R.M., 2006. Greenhouse world and the Mesozoic ocean. Oceanography 19 (4), 64–74.

Takashima, R., Nishi, H., Yamanaka, T., Tomosugi, T., Fernando, A.G., Tanabe, K., Moriya, K., Kawabe, F., Hayashi, K., 2011. Prevailing oxic environments in the Pacific Ocean during the mid-Cretaceous oceanic anoxic event 2. Nature Commun. 2 (234). DOI: 10.1038/ncomms1233.

Tarduno, J.A., Brinkman, D.B., Renne, P.R., Cottrell, R.D., Scher, H., Castillo, P., 1998. Evidence for extreme climatic warmth from Late Cretaceous Arctic vertebrates. Science 282, 2241–2244.

Taylor, S.R., McLennan, S.M., 1995. The geochemical evolution of the continental crust. Rev. Geophys. 33 (2), 241–265.

Tegner, C., Storey, M., Holm, P.M., Thorarinsson, S.B., Zhao, X., Lo, C.-H., Knudsen, M.F., 2011. Magmatism and Eurekan deformation in the High Arctic Large Igneous Province: 40Ar-39Ar age of Kap Washington Group volcanics, North Greenland. Earth Planet. Sci. Lett. 303, 203–214.

Tejada, M.L.G., Mahoney, J.J., Duncan, R.A., Hawkins, M.P., 1996. Age and geochemistry of basement and alkalic rocks of Malaita and Santa Isabel, Solomon Islands, southern margin of Ontong Java Plateau. J. Petrol. 37, 361–394.

Thurow, J., Brumsack, H.-J., Rullkötter, J., Littke, R., Meyers, P., 1992. The Cenomanian/Turonian boundary event in the Indian Ocean—A key to understand the global picture, in: Duncan, R.A., Rea, D.K., Kidd, R.B., von Rad, U., Weissel, J.K. (Eds.), Synthesis of Results from Scientific Drilling in the Indian Ocean, Geophysical Monograph Series. American Geophysical Union, Washington, Vol. 70, pp. 253–273.

Torsvik, T.H., Tucker, R.D., Ashwal, L.D., Eide, E.A., Rakotosolofo, N.A., de Wit, M.J., 1998. Late Cretaceous magmatism in Madagascar: palaeomagnetic evidence for a stationary Marion hotspot. Earth Planet. Sci. Lett. 164, 221—232.

Trabucho-Alexandre, J., Tuenter, E., Henstra, G.A., van der Zwan, K.J., van de Wal, R.S.W., Dijkstra, H.A., de Boer, P.L., 2010. The mid-Cretaceous North Atlantic nutrient trap: black shales and OAEs. Paleoceanography 25 (4), PA4201.

Tribovillard, N., Algeo, T.J., Lyons, T., Riboulleau, A., 2006. Trace metals as paleoredox and paleoproductivity proxies: An update. Chem. Geol. 232, 12—32.

Tsikos, H., Jenkyns, H.C., Walsworth-Bell, B., Petrizzo, M.R., Forster, A., Kolonic, S., Erba, E., Premoli Silva, I., Baas, M., Wagner, T., Sinninghe Damsté, J.S., 2004. Carbon-isotope stratigraphy recorded by the Cenomanian–Turonian Oceanic Anoxic event; correlation and implications based on three key localities. J. Geol. Soc. 161, 711–719.

Turgeon, S.C., Brumsack, H.-J., 2006. Anoxic vs dysoxic events reflected in sediment geochemistry during the Cenomanian–Turonian Boundary Event (Cretaceous) in the Umbria–Marche Basin of central Italy. Chem. Geol. 234, 321–339.

Turgeon, S.C., Creaser, R.A., 2008. Cretaceous oceanic anoxic event 2 triggered by a massive magmatic episode. Nature 454, 323–326.

Tyson, R.V., Pearson, T.H., 1991. Modern and Ancient Continental Shelf Anoxia: An Overview, in: Modern and Ancient Continental Shelf Anoxia. Geol. Soc. Spec. Publ. 58, pp. 1–24.

Van Cappellen, P., Ingall, E.D., 1994. Benthic phosphorus regeneration, net primary production, and ocean anoxia: A model of the coupled marine biogeochemical cycles of carbon and phosphorus. Paleoceanography 9 (5), 677–692.

Vishnevskaya, V.S., 2001. Jurassic and Cretaceous Radiolarian Biostratigraphy of Russia [in Russian]. GEOS, Moscow.

Wan, X., Wignall, P.B., Zhao, W., 2003. The Cenomanian-Turonian extinction and oceanic anoxic event: evidence from southern Tibet. Palaeogeogr. Palaeoclimatol. Palaeoecol. 199, 283–298.

Wang, X., Reinhard, C.T., Planavsky, N.J., Owens, J.D., Lyons, T.W., Johnson, T.M., 2016. Sedimentary chromium isotopic compositions across the Cretaceous OAE2 at Demerara Rise Site 1258. Chem. Geol. 429, 85–92.

Westermann, S., Caron, M., Fiet, N., Fleitmann, D., Matera, V., Adatte, T., Föllmi, K.B., 2010. Evidence for oxic conditions during oceanic anoxic event 2 in the northern Tethyan pelagic realm. Cretaceous Res. 31, 500–514.

Wignall, P.B., 2001. Large igneous provinces and mass extinctions. Earth Sci. Rev. 53, 1–33.

Zakharov, Yu.D., Smyshlyaeva, O.P., Popov, A.M., Shigeta, Ya., 2006. The Stable Isotope Composition of Late Mesozoic Organic Carbonates in the Russian Far East [in Russian]. Dal'nauka, Vladivostok.

Zheng, X.-Y., Jenkyns, H.C., Gale, A.S., Ward, D.J., Henderson, G.M., 2013. Changing ocean circulation and hydrothermal inputs during ocean anoxic event 2 (Cenomanian–Turonian): Evidence from Nd-isotopes in the European shelf sea. Earth Planet. Sci. Lett. 375, 338–348.

Editorial responsibility: N.L. Dobretsov